frontiers | Frontiers in Earth Science

TYPE Original Research
PUBLISHED 12 May 2023
DOI 10.3389/feart.2023.1153415

OPEN ACCESS

EDITED BY
Gilad Antler,
Ben-Gurion University of the Negev, Israel

REVIEWED BY
Elan Levy,
Geological Survey of Israel, Israel
Maya Lorraine Gomes,
Johns Hopkins University, United States
Sydney Riemer,
Yale University New Haven, United States

*CORRESPONDENCE
Jörn Peckmann,
joern.peckmann@uni-hamburg.de

RECEIVED 29 January 2023
ACCEPTED 02 May 2023
PUBLISHED 12 May 2023

CITATION
Rouwendaal SE, Birgel D, Grossi V, Aloisi G, Guibourdenche L, Labrado AL, Brunner B, Rouchy J-M and Peckmann J (2023), Two modes of gypsum replacement by carbonate and native sulfur in the Lorca Basin, SE Spain. *Front. Earth Sci.* 11:1153415. doi: 10.3389/feart.2023.1153415

Two modes of gypsum replacement by carbonate and native sulfur in the Lorca Basin, SE Spain

Simon E. Rouwendaal[1], Daniel Birgel[1], Vincent Grossi[2], Giovanni Aloisi[3], Laetitia Guibourdenche[3], Amanda L. Labrado[4], Benjamin Brunner[4], Jean-Marie Rouchy[5] and Jörn Peckmann[1]*

[1]Institut für Geologie, Centrum für Erdsystemforschung und Nachhaltigkeit, Universität Hamburg, Hamburg, Germany, [2]Laboratoire de Géologie de Lyon (LGL-TPE), Centre National de la Recherche Scientifique (CNRS), Université de Lyon, Lyon, France, [3]Université Paris Cité, Institut de Physique du Globe de Paris, Centre National de la Rechereche Scientifique (CNRS), Paris, France, [4]Department of Earth, Environment and Resource Sciences, The University of Texas at El Paso, El Paso, TX, United States, [5]Departement Origines et Evolution, Paris, France

Organoclastic sulfate reduction and bacterial sulfide oxidation have been suggested to explain the formation of authigenic carbonate and native sulfur replacing gypsum in the Lorca Basin, Spain. To gain more insight into the nature of this replacement, two types of sulfur-bearing carbonate (laminated and brecciated) from the late Miocene Lorca Basin were studied. Petrographic observations revealed that a sulfur-bearing laminated carbonate consists of clay-rich and dolomite-rich laminae with carbonate and native sulfur pseudomorphs after gypsum. Positive $\delta^{18}O_{carbonate}$ values in the laminae ($\delta^{18}O$ = 2.6‰) and lipid biomarkers of halophilic archaea (e.g., extended archaeol) suggest formation under hypersaline conditions. Bacterial sulfate reduction, evidenced by biomarkers such as *iso*-C_{15}, *iso*-C_{16}, and *iso*-C_{17} fatty acids, produced hydrogen sulfide inducing the abiotic formation of organic sulfur compounds. Gypsum in the laminated carbonate likely dissolved due to undersaturation as evidenced by a low content of carbonate-associated sulfate (3,668 ppm) and ^{34}S-enriched native sulfur ($\delta^{34}S$ = 22.4‰), reflecting sulfate limitation. Such ^{34}S-enrichment implies limited fluid flow, which probably restricted the supply of molecular oxygen required for native sulfur formation through oxidation of hydrogen sulfide. Alternatively, sulfate-reducing bacteria may have mediated native sulfur formation directly as a stress response to environmental conditions. The formation of sulfur-bearing calcite in brecciated carbonates is due to post-depositional alteration. Negative $\delta^{18}O$ values of the calcite ($\delta^{18}O$ = −1.5‰) and a tenfold decrease in carbonate-associated sulfate content (752 ppm) suggest gypsum dissolution and subsequent calcite precipitation from meteoric water. Relatively ^{34}S-depleted native sulfur ($\delta^{34}S$ = 13.1‰) leaves it ambiguous whether meteoric water influx could have supplied sufficient molecular oxygen for oxidation of hydrogen sulfide. In case of the brecciated carbonate, methanogenesis, anaerobic oxidation of methane, and bacterial sulfate reduction apparently mediated the formation of secondary minerals as indicated by ^{13}C-depleted lipid biomarkers representative for the respective metabolisms. This study reveals that the conditions and timing of gypsum replacement are variable—taking place 1) during or shortly after gypsum deposition or 2) significantly after sedimentation—and suggests that methanogens in addition to anaerobic methanotrophic archaea and

sulfate-reducing bacteria may be involved in the mineral-forming processes in the sedimentary subsurface.

KEYWORDS

carbonate authigenesis, lipid biomarkers, bacterial sulfate reduction, methanogenesis, anaerobic oxidation of methane, Lorca basin

1 Introduction

Sulfate-bearing evaporitic deposits, such as gypsum or anhydrite, are commonly associated with replacement by authigenic carbonates and native sulfur. These replacement rocks are found in salt dome cap rocks, for instance in the coastal salt domes in the Gulf of Mexico, United States (Feely and Kulp, 1957; Caesar et al., 2019), or as stratabound deposits, like in the Messinian evaporites of Sicily (Hunt, 1915; Dessau et al., 1962; Ziegenbalg et al., 2010; 2012). The sulfur-bearing carbonates of the Lorca Basin in southeastern Spain replace gypsum layers in sedimentary rocks recording alternating periods of basin restriction and opening during the late Miocene (Russell et al., 1997; Rouchy et al., 1998). During basin restriction, abundant gypsum precipitated due to evaporation of seawater, while shales and diatomites, both rich in organic matter deposited during periods of open marine conditions with high primary productivity (Benali et al., 1995; Rouchy et al., 1998; Krijgsman et al., 2000; Drake et al., 2015). Shortly after deposition, the majority of gypsum was replaced by sulfur-bearing carbonates in the Lorca Basin (Rouchy et al., 1998; Andreetto et al., 2019), comprising six to eight layers of sulfur-bearing carbonate (Rouchy et al., 1998; Andreetto et al., 2019).

Gypsum dissolves under a range of environmental conditions (e.g., meteoric water influx, undersaturation of solution) to release calcium (Ca^{2+}) and sulfate ions (SO_4^{2-}). When abundant organic matter, oil, or methane are present, replacement of gypsum by authigenic carbonate and native sulfur formation is typically driven by microbial sulfate reduction. This produces hydrogen sulfide and bicarbonate (HCO_3^-), the latter raising alkalinity and causing secondary carbonate precipitation, which is frequently represented by pseudomorphs after gypsum (Feely and Kulp, 1957; Davis and Kirkland, 1970; Anadon et al., 1992; Peckmann et al., 1999; Ziegenbalg et al., 2010; 2012; Aloisi et al., 2013). Alternatively, at temperatures above 100°C, abiogenic 'thermochemical' sulfate reduction is thought to degrade gypsum in a similar, yet abiotic fashion (Machel et al., 1995). However, the sediments in the Lorca Basin are immature and have therefore not experienced sufficiently high enough temperatures for thermochemical sulfate reduction (Benali et al., 1995; Machel, 2001; Permanyer et al., 2016).

Microbially-mediated, authigenic carbonate formation is inferred from characteristically low $\delta^{13}C_{carbonate}$ values reflecting organic matter remineralization by heterotrophic sulfate-reducing bacteria (SRB, Ziegenbalg et al., 2010; Lindtke et al., 2011), oil-degradation (Aloisi et al., 2013), anaerobic oxidation of methane (AOM, Ziegenbalg et al., 2010), or mixed oil-degradation and AOM (Caesar et al., 2019). The sulfur-bearing carbonates replacing gypsum in the Lorca Basin have been suggested to result from organoclastic sulfate reduction (i.e., oxidation of low molecular weight organic compounds by sulfate-reducing bacteria; Andreetto et al., 2019), most likely fueled by organic matter from organic-rich shales and diatomites in the basin (Russell et al., 1997; Rouchy et al., 1998).

The microbial communities involved in these processes have been additionally characterized by molecular fossils. In case of some Messinian carbonates, characteristic lipids with extreme ^{13}C-depletion were interpreted as biomarkers of anaerobic methanotrophic archaea (ANME) living in a syntrophic partnership with SRB (Ziegenbalg et al., 2012), much like the microbial communities found at marine methane seeps (Niemann and Elvert, 2008). Lipid biomarker data from oil-soaked carbonates rather pointed to oil degradation by SRB, with compounds including uncommon bacterial macrocyclic ether lipids (Baudrand et al., 2010; Aloisi et al., 2013). In samples from the German Zechstein, fatty acid patterns revealed that bacterial sulfate reduction was involved in the precipitation of diagenetic sulfur-bearing aragonite (Peckmann et al., 1999). Although SRB have to date not been recognized by lipid biomarkers for the Lorca Basin, abundant sulfurized organic compounds have been interpreted as evidence of abundant sulfate reduction (Benali et al., 1995; Russell et al., 1997, Russell er al., 2000; Rouchy et al., 1998). Indeed, organic sulfur compounds form when reduced sulfur species are present and when concentrations of metal ions are sufficiently low (especially Fe^{2+}; for reviews see Werne et al., 2004; Amrani, 2014; Kutuzov et al., 2020).

The formation of native sulfur associated with carbonate replacement of sulfate minerals is commonly explained by the abiotic or biological oxidation of hydrogen sulfide in the presence of molecular oxygen (Machel, 1992; Andreetto et al., 2019). However, sulfur isotope analyses of gypsum, native sulfur, barite, celestine, and carbonate-associated sulfate (CAS) revealed that fluid flow in some sulfur deposits was too restricted to supply adequate amounts of molecular oxygen to convert hydrogen sulfide to native sulfur during diagenesis (cf. Labrado et al., 2019). The sulfur isotope offset ($\Delta^{34}S$) between the most ^{34}S-enriched CAS and the most ^{34}S-depleted native sulfur subsequently reflects the ^{34}S-fractionation by microbial sulfate reduction, ranging from 0‰ to as large as 70‰ (e.g., Brunner and Bernasconi, 2005; Sim et al., 2011). Several alternative mechanisms for native sulfur formation other than oxidation of hydrogen sulfide with molecular oxygen have been proposed, all involving anaerobic processes driven by archaea and bacteria or various symbiotic partnerships (Labrado et al., 2019; Amend et al., 2020).

The Lorca Basin is ideal to study the various microbial activities and the potential mechanisms involved in the formation of sulfur-bearing carbonate because several types of sulfur-bearing carbonates with varying mineralogies and textures were found (Russell et al., 1997; Rouchy et al., 1998; Andreetto et al., 2019). To study the biogeochemistry of the Lorca Basin secondary carbonates in more

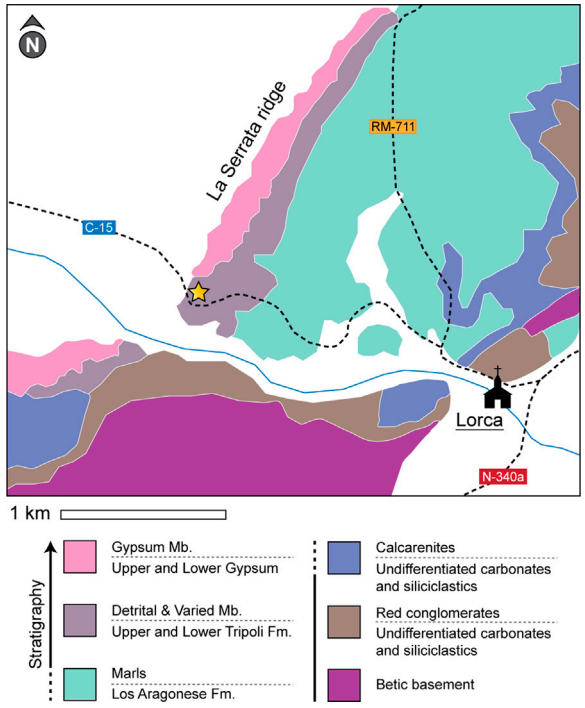

FIGURE 1
Geological map of the Lorca Basin (modified after Garcia-Veigas et al., 2020). White areas are covered by Quaternary alluvium. Star symbol indicates sample location. Lithologies are shown with two names, based on either a Tortonian age (upper name, Garcia-Veigas et al., 2020) or a Messinian age (lower name, Carpentier et al., 2020). "Fm." and "Mb." are abbreviations for Formation and Member.

detail, a multi-disciplinary approach is used on two types of sulfur-bearing carbonates, laminated and brecciated carbonates. Petrography, carbon, oxygen, and sulfur stable isotope analyses were performed to decipher the geochemical processes leading to the formation of such carbonates. Lipid biomarker and their compound-specific carbon isotope analysis were used to investigate which microbial processes were involved in the formation of gypsum-replacing carbonate.

2 Geological setting

The late Miocene Lorca Basin is located in the Betic Cordillera in southeastern Spain. The Betic Cordillera is an ENE-WSW oriented orogenic complex that resulted from the collision between the Iberian and African plates (de Galdeano, 1990). It contains several basins similar to the Lorca Basin. The basins are oriented parallel to the orogenic belt and are separated from each other by similarly oriented ranges of Betic basement rocks. During the late Miocene, these basins experienced progressive restriction, isolation, and eventually continental conditions (Rouchy et al., 1998; Krijgsman et al., 2000). The rock record of the transition from open marine conditions to isolation in the Lorca Basin is represented by sedimentary rocks outcropping at the NE-SW trending ridge of hills called La Serrata (Figure 1). A series of marls, organic-rich shales, and diatomites reflects the marine periods in a semi-enclosed intramontane basin typified by high productivity. Periods of increased basin restriction led to the deposition of intercalated gypsum layers in the sediment series, indicating evaporation and hypersalinity. On top of the succession are two thick evaporitic units of halite and gypsum, respectively, which represent the final stage of basin isolation (Garcia-Veigas et al., 1994; Garcia-Veigas et al., 1995).

The age of the rocks in the Lorca Basin is a matter of debate. The respective lithologies carry different names (see Figure 1) based on age interpretation and correlation with other rocks. Rouchy et al. (1998) and more recently Carpentier et al. (2020) attributed a late Messinian age to the succession based on biostratigraphic and lithostratigraphic analysis. Both groups of authors argued that the sediment series and thick evaporites in the Lorca Basin deposited during the Messinian Salinity Crisis, a period typified by widespread deposition of similar successions in the Mediterranean Sea (Roveri et al., 2014; Andreetto et al., 2021). The sediments below the thick evaporitic units are believed to correlate with similar pre-evaporitic sediments found throughout the Mediterranean and are therefore referred to as Upper and Lower Tripoli Formation (Rouchy, 1982; García-Veigas et al., 1995). Krijgsman et al. (2000) on the other hand argued for a "Tortonian Salinity Crisis" in the eastern Betic Cordillera based on an integrated magnetostratigraphic, biostratigraphic, and cyclostratigraphic study of the Lorca Basin and another nearby basin. García-Veigas et al. (2020) also argued in favor of a Tortonian age, analyzing the geochemistry on the evaporites of the Lorca and the nearby Fortuna Basin, matching the age of evaporites in the nearby Las Minas and Cenajo Basins (Pineda et al., 2021). Both Krijgsman et al. (2000) and Kleikemper et al., 2004 dated the pre-evaporitic succession, named La Serrata Formation, as late Tortonian. This succession is subdivided into the Detrital Member and the Varied Member (Figure 1).

3 Materials and methods

Sulfur-bearing carbonates were sampled at the south end of the La Serrata ridge (Figure 1). The sample of laminated carbonate was collected *in situ* from an outcrop adjacent to the road C-15 (37°41′23.1″N, 1°44′10.7″W), though its stratigraphic position within the pre-evaporitic sediments could not be determined accurately due to poor outcrop conditions. Two similar samples of brecciated carbonate (1 and 2) were collected from mining dumps (37°41′23.9″N, 1°44′03.6″W; Table 1). Throughout the pre-evaporitic succession, several intercalated layers of gypsum-replacing carbonate layers are found. The brecciated carbonates derive from either gypsum-replacing carbonate layer 3 or 4 in the lower part of the succession. These layers were historically mined for sulfur and thus produced the mining dumps (Rouchy et al., 1998). The brecciated (1) carbonate sample failed to produce reliable compound-specific carbon isotope results for the alcohol compounds (see Results below). Though, some of the compounds in the alcohol fraction are crucial for the interpretation of secondary carbonate formation in the brecciated carbonates (see Discussion below). Therefore, the sulfur-bearing cement and cement-filled cavities (i.e., the secondary carbonate) were specifically selected

TABLE 1 Carbon, oxygen, and sulfur isotope compositions of individual carbonate phases, carbonate-associated sulfate (CAS) content, and mineralogy. Carbon and oxygen isotope values are in ‰ vs. V-PDB, sulfur isotope values are in ‰ vs. V-CDT.

Sample	Lithology	$\delta^{13}C$	$\delta^{18}O$	$\delta^{34}S_{CAS}$	CAS (ppm)	$\delta^{34}S_{sulfur}$	XRD (qualitative)
Laminated	dolomite-rich	−7.0	2.6	40.7	3,668	22.4	Dolomite
	clay-rich	−6.8	2.2	40.1	3,669		
Brecciated (1)	clast	−10.3	2.3	35.5	7,121	13.1	Low-Mg calcite, dolomite, quartz
	(micro)sparite	−17.8	−1.0	54.3	752		
	cavity	−15.8	−1.5				
Brecciated (2)	calcite	−18.9	−1.2				Calcite, dolomite, quartz, sulfur

and largely separated from the sedimentary clasts in the brecciated (2) carbonate sample to repeat this analysis.

Thin sections were prepared and partially stained with a combined potassium ferricyanide and alizarin red solution to distinguish calcite from dolomite (Füchtbauer, 1988). Petrography was performed with both cross-polarized and plane-polarized light on a Zeiss Axio Scope.A1 microscope mounted with a Canon EOS 1300D camera. Mineralogy was qualitatively determined for the laminated and brecciated (1) carbonate with a Stoe Stadi MP X-ray diffraction (XRD) system (Mo Kα radiation) at the Mineralogical-Petrographic Institute of the Universität Hamburg. The brecciated (2) carbonate sample was analyzed using a Siemens D-500 powder diffractometer (Ni filtered Cu Kα radiation) at the Laboratoire de Géologie of the University of Lyon.

Different textural phases in the brecciated (1) and laminated carbonate were subsequently drilled with a hand-held microdrill. The powders were analyzed for carbon and oxygen stable isotopes at the MARUM stable isotope laboratory of the University of Bremen. Measurements were performed on a ThermoFisher Scientific 253plus gas isotope ratio mass spectrometer with a Kiel IV automated carbonate preparation device. The analytical error over the measurement period for the in-house Solnhofen limestone standard was 0.03‰ for $\delta^{13}C$ and 0.06‰ for $\delta^{18}O$ values. The in-house standard was calibrated against a NBS 19 calcite standard. All carbon and oxygen stable isotope values are reported in per mil relative to Vienna Pee Dee Belemnite (V-PDB). Oxygen isotope values of carbonate with dominant dolomite mineralogy were not corrected because of an undetermined admixture of minor calcite (Sharma and Clayton, 1965). For the carbon and oxygen stable isotope analysis of the brecciated (2) sample, a semi-automated online method as described by Baudrand et al. (2012) and Aloisi et al. (2013) was used. Relative amounts of calcite and dolomite were quantified with the MacDiff program using the X-ray diffraction data. Dolomite and calcite contents were calculated by combining the relative quantification with carbonate content measurements from a Mélières manocalcimeter. Calcite and bulk carbonate stable isotope compositions were measured with an auto sampler MultiPrep™ system coupled to a Dual-Inlet GV- isotope ratio mass spectrometer at the Laboratoire de Géologie of the University of Lyon. The standard deviation of the measurement was calculated as described in Baudrand et al. (2012). The error for the calcite stable isotope measurement was less than 0.10‰ for $\delta^{13}C$ and 0.10‰ for $\delta^{18}O$ values.

For the analysis of carbonate-associated sulfate (CAS) content and sulfur isotopes, different textural phases from the laminated carbonate and brecciated (1) carbonate were separated and were grinded manually to a fine powder. The powders were soaked overnight with a sodium chloride solution to remove easily soluble sulfate. Hydrochloric acid was added to dissolve the remaining carbonate. After dissolution, CAS was precipitated as barium sulfate by adding barium chloride to the acid insoluble residue (see Gischler et al., 2020). Content and isotope measurements were performed on an Elemental Analyzer (Elementar Pyro Cube) coupled to an isotope ratio mass spectrometer (Elementar GeoVisION) at the University of Texas at El Paso. The standard error (σ) was less than 0.30‰ for $\delta^{34}S$ values, based on repeated analyses of in-house and international standards. For the sulfur isotope measurements of native sulfur, solid sulfur from carbonate samples was extracted as Cu_xS_x using heptane and activated copper repeatedly. Cu_xS_x was then reduced into H_2S using acidic chromium reducible solution, prepared following the procedure of Fossing and Jørgensen (1989). The product H_2S was transformed into Ag_2S by reacting with a $AgNO_3$ solution (Geng et al., 2018), rinsed three times with MilliQ water and finally dried in an oven at 60°C. Ag_2S powder was subsequently reacted with F_2 to produce gaseous SF_6, purified (cryogenically and chromatographically) and analyzed by a dual inlet mass spectrometer MAT-253 at the Institut de Physique du Globe de Paris of Université Paris-Cité (Ono et al., 2006; Labidi et al., 2012). The $\delta^{34}S$ values were calibrated with an in-house SF_6 standard using IAEAS-1 international standard that has a $\delta^{34}S$ value of −0.31‰ V-CDT (Brand et al., 2014). Repeated analyses of IAEAS-1 yield $\delta^{34}S$ = −0.31‰ ± 0.2. All sulfur isotope measurements are reported as ‰ relative to Vienna-Canyon Diablo Troilite (V-CDT).

Preparation, decalcification, and extraction of lipid biomarkers for the laminated carbonate and the brecciated (1) carbonate followed the procedure described in Thiel et al. (1999), Birgel et al. (2006), and Sabino et al. (2020). The surfaces of the samples were removed, the remaining samples (188 g and 210 g) were crushed and carefully cleaned with acetone and 10% hydrochloric acid. The samples were subsequently dissolved with 10% hydrochloric acid. For each sample, the residual sediment was saponified with 6% KOH in methanol (MeOH) in a 50 ml screwcap vial in an ultrasonic bath at 80°C for 2 h. Lipids were extracted from the saponified sediment by repeated ultrasonication with dichloromethane (DCM):MeOH (3:1, v/v), until the solvent was

colorless. The total lipid extract was then transferred to a separatory funnel and MilliQ water was added; to ensure the transfer of all fatty acids into the organic phase, pH was kept constant at 2 by adding 10% hydrochloric acid. The DCM phase containing the total lipid extract was repeatedly extracted from the funnel by adding new DCM and repeating the process. The total lipid extract was dried and then split into a *n*-hexane-soluble fraction (maltenes) and DCM-soluble fraction (asphaltenes). Elemental sulfur was removed overnight by adding activated Cu to the maltene fraction, which was further split into four fractions of increased polarity (hydrocarbons, ketones, alcohols, fatty acids) using column chromatography (SPE Chromabond, NH_2, 6 ml/500 mg). Half of the alcohol fraction was derivatized for 2 h at 80°C by adding pyridine and N,O-bis(trimethylsilyl)trifluoroacetamide (BSTFA; 1:1, v/v). The fatty acid fraction was derivatized for 1 h at 70°C by adding 10% borium trifluoride (BF_3) in MeOH. Fatty acids were subsequently extracted by adding *n*-hexane and MilliQ water and removing the organic supernatant. The underivatized part of the alcohol fraction was treated with hydrogen iodide and reduced with $LiAlH_4$ (cf. Birgel et al., 2014) to cleave ether bonds and release the side chains of archaeal and bacterial lipids, such as glycerol dibiphytanyl glycerol tetraethers (GDGTs) and isoprenoidal and non-isoprenoidal dialkyl glycerol diethers (DAGEs). The asphaltene fraction was desulfurized to release sulfurized compounds from organic macromolecules formed by intermolecular sulfurization (see Discussion for further explanation). The detailed desulfurization procedure was described in Sabino et al. (2020). The resulting hydrocarbons were separated from the remaining polar compounds with a silica gel column.

Lipid biomarkers were identified using a Thermo Scientific Trace GC Ultra gas chromatograph coupled to a Thermo Scientific DSQ II mass spectrometer; biomarkers were quantified using a Thermo Scientific Trace GC 1310 with a flame ionization detector. Both GCs used a 30 m DB-5MS ultra inert fused silica capillary column with a diameter of 0.25 mm and a film thickness of 0.25 µm. The GC temperature program was set to 50°C (held for 3 min) ramping up to 230°C at 5°C min^{-1}, and then to 325°C (held for 25 min) at 6°C min^{-1}. Compound-specific carbon isotope analysis was performed using an Agilent 6890 GC coupled sequentially to a Thermo Finnigan Combustion III interface and a Thermo Finnigan Delta Plus isotope mass spectrometer (GC-IRMS). The same column and temperature program as described above were used for the isotope measurements. $\delta^{13}C$ values are reported in ‰ relative to V-PDB and were corrected for derivatization. The error of the $\delta^{13}C$ values is less than 1‰. The $\delta^{13}C$ values for the compounds in the alcohol fractions are reported only as ether cleavage products due to the high sulfur contents in this fraction, which compromised isotope measurements.

The brecciated (2) carbonate sample was extracted and separated as described in Baudrand et al. (2010) and Aloisi et al. (2013). The surface of the sample was taken away and the remaining sample was cleaned with acetone and subsequently ground manually in a mortar. Lipid biomarkers were extracted two times with MeOH, two times with DCM:MeOH (1:1, v/v), and finally two times with DCM using ultrasonication. Elemental sulfur was removed overnight by adding activated Cu to the extract. The extract was split into an apolar and a polar fraction by adsorption chromatography over a wet packed column of silica gel (4% H_2O). An aliquot of the polar fraction was derivatized for 1 hour at 60°C by adding pyridine and BSTFA (2:1, v/v). Lipid biomarker analysis was performed using GC-MS at the Laboratoire de Géologie of the University of Lyon. Lipid biomarkers were identified with a HP6890 GC interfaced to either a MD800 Voyager or an Agilent 5975C MS. The GC was equipped with the same column as described for the laminated and brecciated 1) carbonate. The GC temperature program was set to 60°C (held for 1 min), ramping up to 130°C at 20°C min^{-1}, and then to 320°C (held for 30 min) at 4°C min^{-1}. Compound-specific carbon isotope analysis was performed using either a Thermo MAT253 GC-irms (Pancost and Pagani, 2006), or a HP7890B gas chromatograph coupled to an Isoprime visION isotope ratio mass spectrometer via a GC-5 combustion interface at the Laboratoire de Géologie of the University of Lyon. The same column and temperature program as described above were used for the isotope measurements. All $\delta^{13}C$ values are reported in ‰ relative to V-PDB and are corrected for derivatization. Errors for $\delta^{13}C$ values were typically less than 1‰.

4 Results

4.1 Petrography, X-ray diffraction and stable isotopes

4.1.1 Laminated carbonate

The laminated Lorca carbonate shows irregular, wrinkly lamination, with laminae that vary in vertical thickness from half a millimeter to a centimeter. Lamination is horizontally continuous. The laminae are alternating between clay-rich and dolomite-rich (Figures 2A,B) and are not bioturbated. The dolomite laminae consist of microcrystalline dolomite and sparitic dolomite with local peloidal fabrics. Peloids are circular and roughly 100 µm up to 400 µm in size (Figure 2B). Both types of laminae contain carbonate pseudomorphs after gypsum (Figures 2A,B). The pseudomorphs range in size from 50 µm up to a few millimeters. The pseudomorphs in the dolomite-rich laminae are µm-sized, while those in the clay-rich laminae can be mm-sized. Pseudomorphs are lenticular, trapezoidal, and lozenge-shaped (Figures 2A,B). The elongated axes of these crystals are generally aligned with the layering. No deformation is apparent around the pseudomorphs. The majority of pseudomorphs consist of microcrystalline dolomite or have rims of dolomite, but large calcite crystals are common too (Figure 2A). Native sulfur and celestine are also solely found as pseudomorphs after gypsum (Figures 2A,B), again lacking evidence of deformation resulting from mineral growth. Native sulfur occasionally envelopes calcite (Figure 2B). The microcrystalline dolomite rims of pseudomorphs frequently enclose calcite, native sulfur, and celestine (Figure 2A).

The carbon stable isotope compositions of carbonate in the laminae rich in microcrystalline dolomite and in the clay-rich laminae are similar ($\delta^{13}C_{dolomite}$ = −7.0‰ and $\delta^{13}C_{clay}$ = −6.8‰), whereas the oxygen stable isotope values show little more variability ($\delta^{18}O_{dolomite}$ = 2.6‰; $\delta^{18}O_{clay}$ = 2.2‰; Table 1). CAS contents in the laminated carbonate are similar with 3,668 ppm and 3,669 for the dolomite-rich and clay-rich laminae, respectively (Table 1) and CAS is enriched in ^{34}S ($\delta^{34}S_{CAS\text{-}dolomite}$ = 40.7‰; $\delta^{34}S_{CAS\text{-}clay}$ = 40.1‰). Native sulfur found in the laminated carbonate is also ^{34}S-enriched, although less than CAS ($\delta^{34}S_{native\ sulfur}$ = 22.4‰).

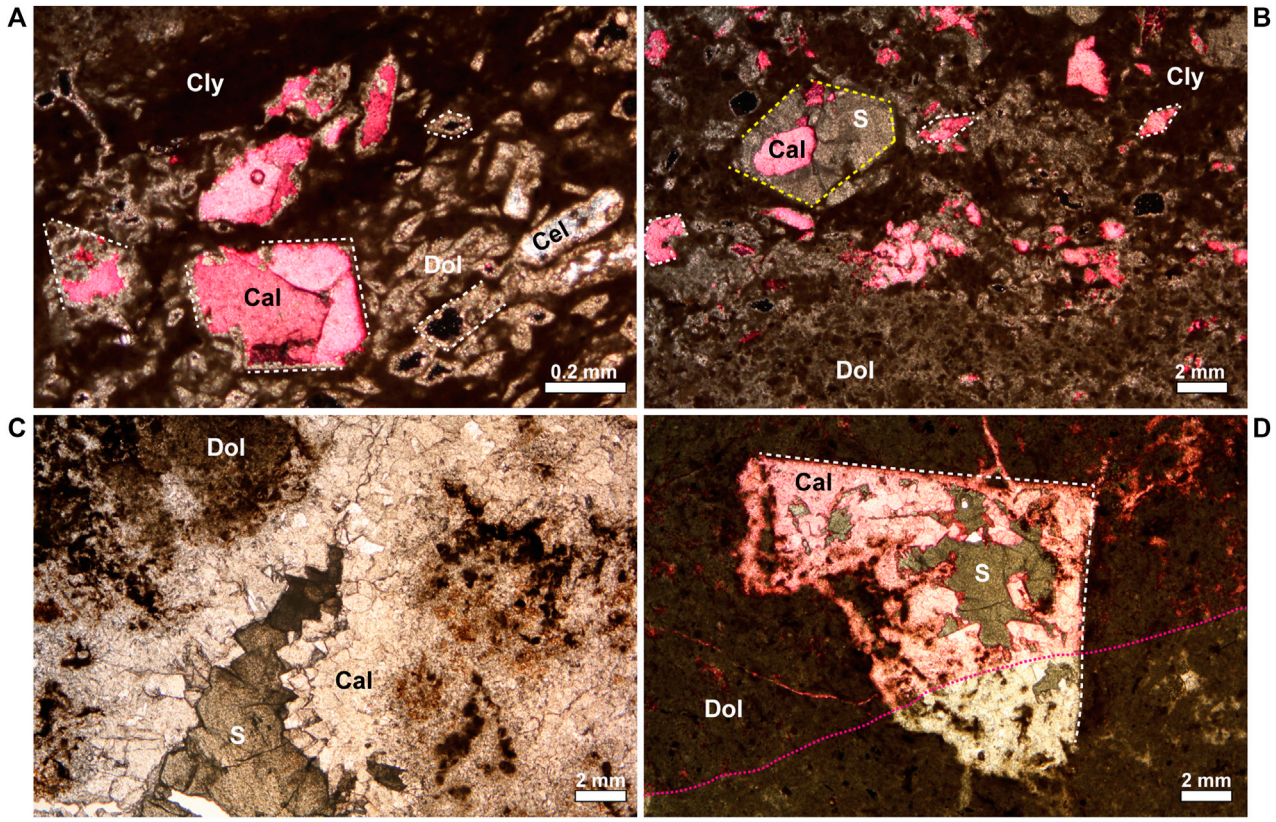

FIGURE 2
Petrography of the laminated **(A, B)** (under cross-polarized light) and brecciated **(C, D)** (under plane-polarized light) carbonates. White dashed lines in A and B delimit pseudomorphs after gypsum with dolomite rims. Yellow dashed lines highlight pseudomorphs after sulfur and sparry calcite. Calcite is stained pink with alizarin red-S. **(C, D)** Brecciated carbonate with peloidal dolomite, microcrystalline dolomite, sparry calcite cement, and sulfur. **(D)** Pseudomorphs after gypsum (white dashed line); calcite is partially stained pink with alizarin red-S (pink dotted line separates the stained from the unstained part of the thin section). Cal = calcite, Dol = dolomite, S = sulfur, Cel = celestine, Cly = clay-rich.

4.1.2 Brecciated carbonates

The brecciated carbonate samples consist of dolomite clasts, calcite cement, and large cavities. The lithology is matrix-dominated and contains clasts varying in size, from a few millimeters up to several centimeters. The fabric of the dolomite clasts is either aphanitic or peloidal (Figures 2C,D). Commonly clasts are crosscut by calcite veins. The clasts have either sharp or blurred boundaries (Figures 2C,D). Sharp clast boundaries probably reflect dissolved gypsum crystals that were adjacent to the clasts. Pseudomorphs after gypsum are abundant (Figure 2D). Pseudomorphs are several millimeters in size and have lenticular, trapezoidal, and lozenge shapes and contain calcite and native sulfur (Figure 2D). Calcite exhibits a (micro)sparitic texture (Figures 2C,D). Crystal growth started from physical boundaries, eventually forming scalenohedral calcite within cavities (Figure 2C). Native sulfur forms millimeter-sized nodules within calcite and cavities (Figures 2C,D). XRD analysis of the brecciated carbonate revealed that main carbonate phase is low-Mg calcite, accompanied by minor amounts of dolomite and quartz.

In the brecciated (1) sample, the calcite of the (micro)sparite texture and the calcite from cavity walls are both ^{13}C-depleted ($\delta^{13}C_{(micro)sparite}$ = −17.8‰; $\delta^{13}C_{cavity}$ = −15.8‰; Table 1). The $\delta^{18}O$ values show little variability ($\delta^{18}O_{(micro)sparite}$ = −1.0‰; $\delta^{18}O_{cavity}$ = −1.5‰). In the peloidal dolomite and clasts of microcrystalline dolomite, carbonate is less ^{13}C-depleted and more ^{18}O-enriched ($\delta^{13}C_{clast}$ = −10.3‰; $\delta^{18}O_{clast}$ = 2.3‰). In the brecciated (2) sample, the values obtained for calcite are similar to those of the (micro)sparite in the brecciated (1) sample ($\delta^{13}C_{calcite(2)}$ = −18.9‰; $\delta^{18}O_{calcite(2)}$ = −1.2‰). CAS contents in the brecciated (1) sample are 752 ppm and 7,121 ppm for the microsparite and the clasts, respectively (Table 1). CAS in the brecciated (1) sample is ^{34}S-enriched, although the value obtained from clasts ($\delta^{34}S_{CAS\text{-}clast}$ = 35.5‰) is significantly lower than the values obtained for microsparite ($\delta^{34}S_{CAS\text{-}microsparite}$ = 54.3‰). Native sulfur is also enriched in ^{34}S, although less than CAS ($\delta^{34}S_{native\ sulfur}$ = 13.1‰).

4.2 Lipid biomarkers and compound-specific carbon isotopes

4.2.1 Laminated carbonate

4.2.1.1 Hydrocarbon fraction

The total amount of hydrocarbons in the laminated carbonate is 3,840 ng/g rock (Supplementary Table S1). Among hydrocarbons, *n*-alkanes comprise 591 ng/g rock and show an odd-over-even

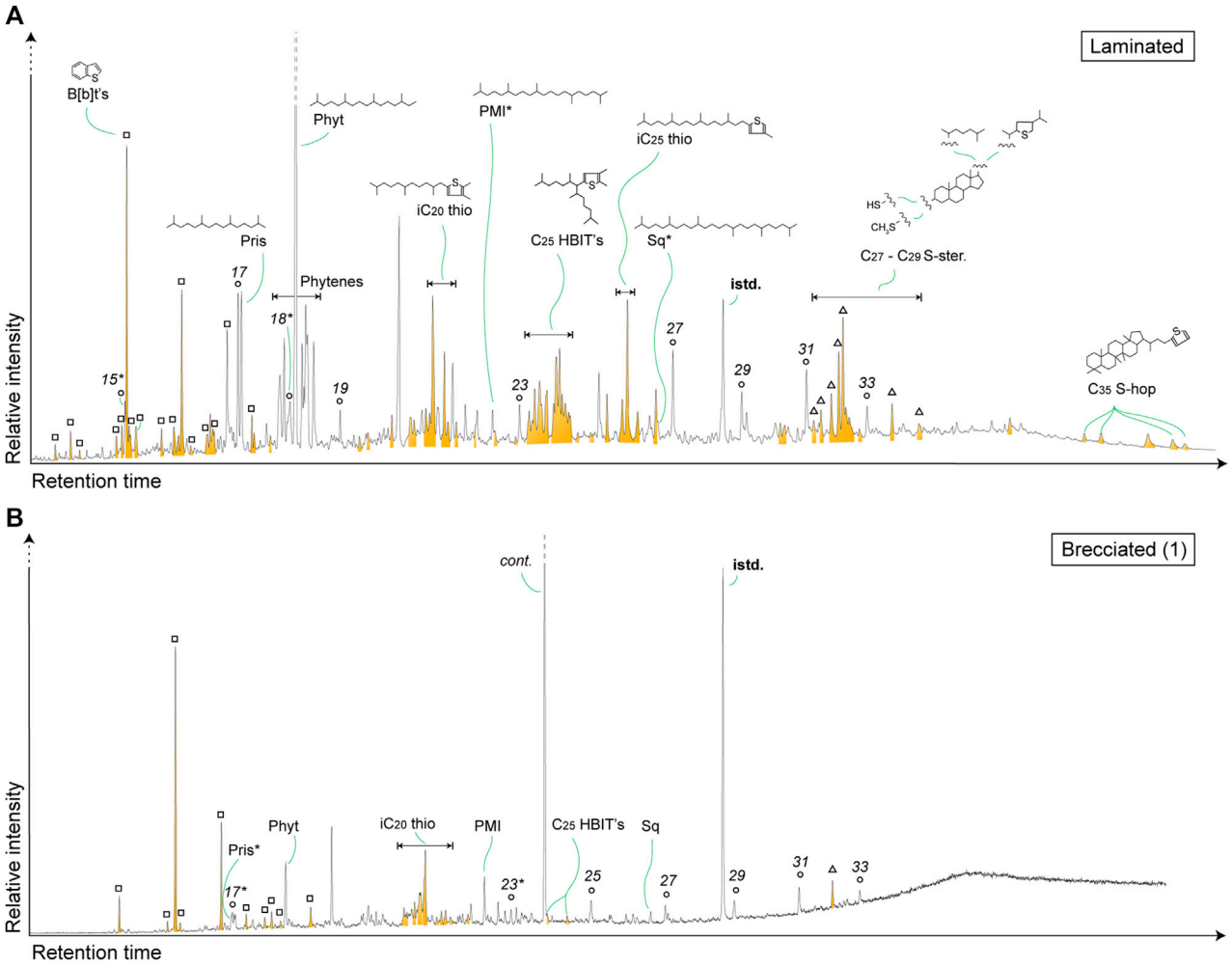

FIGURE 3
Partial gas chromatograms (GC-FID) of hydrocarbon fractions of **(A)** laminated carbonate and **(B)** the brecciated (1) carbonate. Squares indicate benzo[b]thiophenes, circles highlight *n*-alkanes numbered with their corresponding chain length, and triangles indicate sulfurized steranes. Yellow colored peaks correspond to organic sulfur compounds. For selected compounds, molecular structures and names are provided. For steranes, different structural configurations of the found steranes are shown. B[b]t's = benzo[b]thiophenes, Pris = pristane, Phyt = Phytane, iC_{20} thio = phytanyl thiophenes, thiolanes and thianes, iC_{25} thio = PMI thiophenes, C_{25} HBIT's = C_{25} highly-branched isoprenoid thiophenes, thiolanes and thianes, Sq = squalane, C_{27}–C_{29} S-ster. = C_{27}–C_{29} steranes with thiols or thiolanes, C_{35} S-hop = C_{35} thiophene hopanes, istd = internal standard, cont. = contamination. * = co-elution.

predominance. Short-chain *n*-alkanes (C_{15}-C_{24}) are more abundant than long-chain *n*-alkanes (C_{25}-C_{33}), with *n*-C_{17} as most abundant alkane. Isoprenoid hydrocarbons comprise 1,050 ng/g rock, with phytane as most abundant compound (618 ng/g rock). Phytane is accompanied by several unsaturated phytenes. Other, minor isoprenoid hydrocarbons are farnesane, *nor*-pristane, pristane, phytane, 2, 6, 10, 15, 19-pentamethylicosane (irregular PMI; hereafter "PMI" as opposed to 2, 6, 10, 14, 18-pentamethylicosane; hereafter "regular PMI"), and squalane. Other minor hydrocarbons are methyl-trimethyl-tridecyl-chromanes, albeit in low contents (36 ng/g rock in total).

The major lipid group in the hydrocarbon fraction are organic sulfur compounds with total contents of 2,163 ng/g rock (Figure 3A). Organic sulfur compounds in the laminated carbonate mainly comprise various thiophenes, thiolanes, and thianes (cf. Werne et al., 2004; Amrani, 2014; Kutuzov et al., 2020). High amounts of alkyl benzo[b]thiophenes, with a total content of 562 ng/g rock, are also observed (cf. Sinninghe Damsté and de Leeuw, 1990; Kutuzov et al., 2020). Organic sulfur compounds also include isoprenoids, such as various phytane thiophenes and regular PMI thiophenes. Sulfurized highly branched isoprenoids (HBIs), especially C_{25} HBIs, sum up to 422 ng/g rock (cf. Wakeham et al., 1995) and include thiophenes, thiolanes, and thianes. Sulfurized cyclic terpenoids, such as C_{27} to C_{29} steranes thiophenes and thiols (cf. Adam et al., 1991; Behrens et al., 1997), and C_{35} hopane thiophenes (cf. Valisolalao et al., 1984), are found too. The sulfurized steranes are highly abundant, with a total content of 272 ng/g rock, whereas the sulfurized C_{35} hopanes have a content of 53 ng/g rock.

The $\delta^{13}C$ values of the long chain *n*-alkanes vary from −28 to −21‰, whereas the short-chain *n*-alkanes range from −29‰ to −23‰ (Supplementary Table S1; Figure 4). The

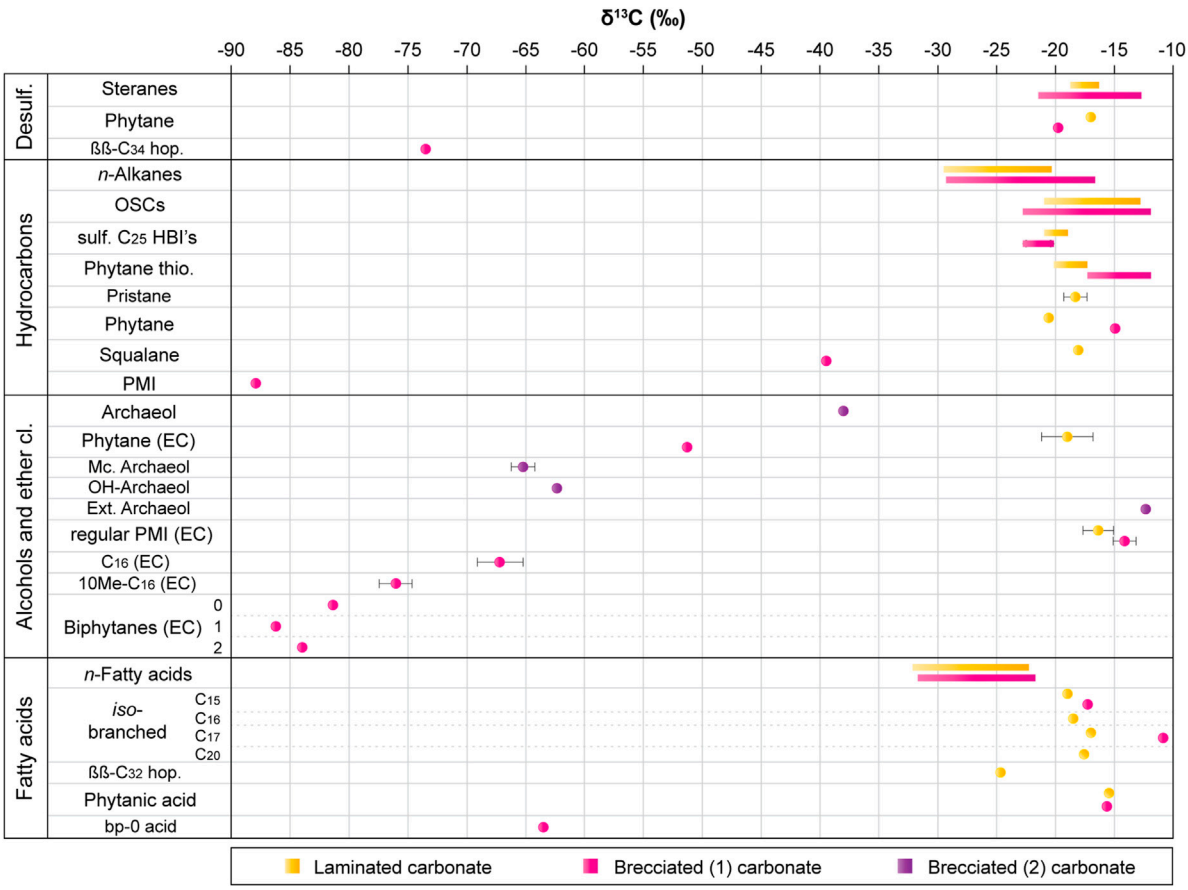

FIGURE 4
Compound-specific carbon isotope composition of selected biomarkers. $\delta^{13}C$ values are in ‰ vs. V-PDB. Colored circles are $\delta^{13}C$ values for specific compounds. Color bars show ranges of values for grouped compounds (e.g., *n*-alkanes). Error bars are shown when $\sigma > 1$. ββ-C_{34} hop. = 17β(H),21β(H)-C_{34} hopane, OSCs = organic sulfur compounds, sulf. C_{25} HBIs = sulfurized C_{25} highly-branched isoprenoids (includes thiophenes, thiolanes and thianes), Phytane thio. = phytane thiophenes, PMI = 2,6,10,15,19-pentamethylicosane, McDGs = macrocyclic dietherglycerols, where A, B and C refer to different moieties (see Results for more details), Mc. Archaeol = macrocylic archaeol, OH-Archaeol = *sn-2* hydroxyarchaeol, Ext. Archaeol = extended archaeol, PMI regular = 2, 6, 10, 14, 18-pentamethylicosane, Biphytanes 0, 1 or 2 = biphytanes with 0, 1 or 2 cyclopentane rings, ββ-C_{32} hop. = 17β(H),21β(H)-C_{32} hopanoic acid, bp-0 acid = acyclic biphytanic acid. EC = compounds released and measured for their isotopes after ether cleavage.

free saturated isoprenoids show $\delta^{13}C$ values ranging from −21‰ to −18‰. Phytane has a $\delta^{13}C$ value of −21‰, $\delta^{13}C$ values of phytenes range from −27‰ to −16‰. The $\delta^{13}C$ value of pristane ($\delta^{13}C$ = −21‰) needs to be interpreted with caution as it partly co-elutes with *n*-C_{17} ($\delta^{13}C$ = −26‰). The organic sulfur compounds have $\delta^{13}C$ values ranging from −21‰ to −13‰. Benzo[b]thiophenes show $\delta^{13}C$ values ranging from −19‰ to −17‰. The $\delta^{13}C$ values of phytane thiophenes range from −20‰ to −18‰, regular PMI thiophenes yielded a value of −18‰ and values of sulfurized HBIs range from −21‰ to −19‰. Neither sterane and hopane thiophenes nor methyl-trimethyl-tridecyl-chromanes yielded $\delta^{13}C$ values due to too low contents.

4.2.1.2 Alcohols and ether cleavage products

The total amount of alcohols in the laminated carbonate is 1,525 ng/g rock, of which 209 ng/g rock are short-chain *n*-alcohols; long-chain alcohols are absent (Supplementary Table S1). Isoprenoid alcohols are most abundant and make up 1,269 ng/g rock. 2,3-diphytanyl-*O*-*sn*-glycerol-diether ($C_{20\text{-}20}$ archaeol) is the most abundant compound in this fraction (893 ng/g rock). 2-*O*-phytanyl-3-*O*-sesterterpanyl-*sn*-glycerol-diether ($C_{20\text{-}25}$ archaeol = extended archaeol) is present in minor amounts of 70 ng/g rock (Supplementary Figure S1). The C_{20} isoprenoid alcohol phytanol was found with 306 ng/g rock. Other compounds are non-isoprenoidal macrocyclic glycerol diethers (McDGs A-C; cf. Baudrand et al., 2010), which are present with low contents.

Due to an unresolved mixture of compounds in the alcohol fractions, compound-specific carbon isotope values of intact compounds were found to be not reliable, therefore their ^{13}C compositions were determined from their ether cleaved hydrocarbon products. Ether cleavage of the underivatized alcohol fraction produced phytane, predominantly derived from cleavage of archaeol, but also from phytanol and partially extended archaeol. This phytane has a $\delta^{13}C$ value of −18‰. Regular PMI, deriving from the cleavage of extended archaeol, has a $\delta^{13}C$ value of −16‰. Acyclic biphytane, which derives from GDGT-0 and GDGT-1, was identified as well, though present in minor amounts (16 ng/g rock). Measurements did not yield a $\delta^{13}C$ value

for acyclic biphytane due to too low contents. Contents of other biphytanes (bicyclic, tricyclic) were too low to be quantified and could not be measured for compound-specific carbon isotope compositions.

4.2.1.3 Fatty acid fraction

The fatty acid fraction yielded by far the highest content of lipid biomarkers summing up to 79.7 µg/g rock, which is about 20 times more than the hydrocarbon and alcohol fractions (Supplementary Table S1). Saturated *n*-fatty acids are the dominant components, with a content of 73.5 µg/g rock and a characteristic even-over-odd predominance. Saturated short-chain *n*-fatty acids (C_{11}-C_{24}) are significantly more abundant than long-chains (C_{25}-C_{32}), with 3.7 µg/g rock against 1.5 µg/g rock. The most abundant saturated *n*-fatty acids are C_{18}, C_{22}, and C_{28} (1.0, 20.0, 1.0 µg/g rock, respectively). A series of terminally branched *iso*- and *anteiso*-fatty acids ranges from C_{13} to C_{20}, with *iso*-C_{15} and *iso*-C_{17} most abundant. The ratio of *anteiso*-/*iso*-fatty acids shows a predominance of *iso*-fatty acids, ranging from 0.14 to 0.28. Only for C_{19}, *anteiso*-fatty acid predominates over *iso*-fatty acid with a ratio of 4.34. Besides terminally branched fatty acids, the mid-branched 10Me-C_{16} fatty acid and a series of isoprenoic fatty acids are present. Among them are farnesic (3, 7, 11-trimethyldecanoic), pristanic (2, 6, 10, 14-tetramethylpentadecanoic), phytanic (3, 7, 11, 15-tetramethylhexadecanoic), and regular PMI acids. Hopanoic acids with chain lengths from C_{31} to C_{35} are present with both 17α(H), 21β(H) and 17β(H), 21β(H) stereoisomers. Further, two C_{18} thiophenic acids were identified (116 ng/g rock and 64 ng/g rock).

Short-chain *n*-fatty acids have $\delta^{13}C$ values ranging from −32‰ to −23‰, and values of long-chain *n*-fatty acids range from −30‰ to −23‰. $\delta^{13}C$ values of *iso*-fatty acids range from −19‰ to −17‰, whereas $\delta^{13}C$ values of *anteiso*-fatty acids could not be obtained due to too low contents. Isoprenoic fatty acids have $\delta^{13}C$ values spanning from −18‰ to −15‰. 17β(H),21β(H)-C_{32} hopanoic acid has a $\delta^{13}C$ value of −25‰.

4.2.1.4 Desulfurized asphaltene fraction

The desulfurized asphaltene fraction contains hydrocarbons released after cleavage of sulfurized macromolecules (see Discussion for further explanation; Supplementary Table S1). Unfortunately, *n*-alkanes could not be reliably investigated due to contamination with *n*-alkanes from the chemical reactant used for desulfurization. Other compounds include isoprenoids (178 ng/g rock) with phytane most abundant (153 ng/g rock). Steranes account for a content of 213 ng/g rock. Phytane from desulfurization has a $\delta^{13}C$ value of −17‰, steranes range from −19‰ to −15‰.

4.2.2 Brecciated carbonates

4.2.2.1 Hydrocarbon fraction

Brecciated (1) carbonate has a total hydrocarbon content of 406 ng/g rock (Supplementary Table S1). Among the hydrocarbons, 88 ng/g rock are *n*-alkanes. The *n*-alkanes reveal odd-over-even dominance for long-chain *n*-alkanes, with *n*-C_{31} as the most abundant *n*-alkane (Figure 3B). No short-to mid-chain *n*-alkanes other than *n*-C_{23} and *n*-C_{24} are present. Isoprenoids have a total content of 73 ng/g rock. Phytane is the most abundant isoprenoid compound with a content of 40 ng/g rock, accompanied by minor amounts of squalane and PMI. As for the laminated carbonate, organic sulfur compounds are the major group in the hydrocarbon fraction of the brecciated (1) carbonate, with a total content of 258 ng/g rock. Benzo[b]thiophenes comprise 132 ng/g rock in total. The brecciated (1) carbonate also contains phytane thiophenes with 60 ng/g rock. Sulfurized HBIs include thiophenes, thiolanes, and thianes, albeit in low abundance (21 ng/g rock) and dominated by C_{20} HBIs. A C_{29} steroid thiolane (Behrens et al., 1997) is present too.

The $\delta^{13}C$ values of the long-chain *n*-alkanes vary from −29‰ to −17‰, with long-chain *n*-alkanes ranging from −29‰ to −21‰ and short-chain *n*-alkanes ranging from −21‰ to −17‰. The $\delta^{13}C$ values for the isoprenoids are −88‰ for PMI, −39‰ for squalane, and −15‰ for phytane. Organic sulfur compounds have values ranging from −23‰ to −12‰. Alkyl benzo[b]thiophenes have $\delta^{13}C$ values ranging from −20‰ to −17‰. Values of phytane thiophenes span from −17‰ to −12‰, those of HBI organic sulfur compounds range from −23‰ to −15‰ and the C_{29} steroid thiolane has a $\delta^{13}C$ value of −16‰.

4.2.2.2 Alcohols and ether cleavage products

The brecciated (1) carbonate yielded 1,455 ng/g rock of alcohol compounds in total (Supplementary Table S1). Among the alcohols, 53 ng/g rock are *n*-alcohols exclusively composed of short-chain *n*-alcohols. Isoprenoid alcohols are the major group of compounds with a total content of 1,273 ng/g rock. Archaeol is the most abundant compound (1,036 ng/g rock). Other isoprenoidal glycerol diethers are present in lesser amounts (Supplementary Figure S1), as, for example, extended archaeol (30 ng/g rock) or macrocyclic archaeol (cf. Comita et al., 1984; 89 ng/g rock) and *sn*2-hydroxyarchaeol ($C_{20,20}$ *sn2*, C-7 hydroxy diphytanyl glycerol diether, 46 ng/g rock). Phytanol is a minor compound (48 ng/g rock). A non-isoprenoidal dialkyl glycerol diether (DAGE) is present in minor amounts (31 ng/g rock). This compound was identified as a C_{36} DAGE (cf. Vinçon-Laugier et al., 2016). The structure was further confirmed after ether cleavage, which yielded a 10Me-C_{16} alkane and a *n*-C_{16} alkane. Other glycerol diethers present are the McDGs A-C (14 ng/g rock, 17 ng/g rock, 21 ng/g rock, respectively).

Due to an unresolved mixture of compounds in the alcohol fraction, compound-specific carbon isotope values of intact compounds were found to be not reliable for the brecciated (1) carbonate sample. Isotope measurements gave reproducible results for the alcohol fraction from the brecciated (2) carbonate sample. $\delta^{13}C$ values were −38‰ for archaeol, −12‰ for extended archaeol, −65‰ for macrocyclic archaeol and −65‰ for *sn*2-hydroxyarchaeol.

Other compounds of the alcohol fraction released after ether cleavage in the brecciated (1) carbonate sample are acyclic, monocyclic, and bicyclic biphytanes with contents of 291 ng/g rock, 31 ng/g rock, and 21 ng/g rock, respectively. The compounds mostly derive from the ether cleavage of GDGT-0 to GDGT-4 (Birgel et al., 2008), although the ether cleavage of macrocyclic archaeol also results in acyclic biphytane. Biphytanes are strongly ^{13}C-depleted, with $\delta^{13}C$ values of −81‰ for acyclic biphytane, −86‰ for monocyclic biphytane, and −84‰ for bicyclic biphytane, suggesting only minor contribution of ether-cleaved biphytane from macrocyclic archaeol, which has a higher $\delta^{13}C$ value of −65‰ (see above).

Ether cleavage of the alcohol fraction from the brecciated (1) sample resulted in regular PMI, deriving from the cleavage of extended archaeol, with a $\delta^{13}C$ value of −14‰. Phytane released after ether cleavage shows a $\delta^{13}C$ value of −51‰. This compound derives from phytanol and isoprenoidal glycerol diethers, with the largest contribution probably deriving from the abundant archaeol. The alkanes released by C_{36} DAGE show $\delta^{13}C$ = −76‰ for 10Me-C_{16} and $\delta^{13}C$ = −67‰ for C_{16}, though the $\delta^{13}C$ of the C_{16} alkane is affected by minor contributions of *n*-C_{16} alcohol.

4.2.2.3 Fatty acid fraction

The fatty acid fraction corresponds to an overall high content of 11.5 μg/g rock (Supplementary Table S1). The saturated *n*-fatty acids are the dominant components, with a content of 10.4 μg/g rock and a characteristic even-over-odd predominance. Saturated long-chain *n*-fatty acids including C_{29} (7.5 μg/g rock) are more abundant than short-chain *n*-fatty acids. Brecciated (1) carbonate yielded a series of terminally branched *iso*- and *anteiso*-fatty acids including C_{15}, C_{16}, and C_{17}. *Anteiso*-predominate over *iso*-fatty acids with a ratio ranging from 0.19 to 0.24. Pristanic, phytanic, and PMI acids as well as biphytanic diacid (bp-0) are present in the brecciated (1) carbonate, with phytanic acid most abundant (881 ng/g rock). $\delta^{13}C$ values of *n*-fatty acids range from −31‰ to −22‰. The most abundant fatty acid, *n*-C_{29}, has a $\delta^{13}C$ value of −22.0‰, while *iso*- and *anteiso*-fatty acids range from −17‰ to −11‰. Other values obtained include −16‰ for phytanic acid and −64‰ for bp-0 acid.

4.2.2.4 Desulfurized asphaltene fraction

The desulfurized asphaltene fraction contains 31 ng/g rock isoprenoids with phytane as most abundant compound (27 ng/g rock; Supplementary Table S1). Other compounds are various steranes, accounting for a content of 114 ng/g rock. Another compound in this fraction is 17β(H), 21β(H)-C_{34} hopane with a content of 6 ng/g rock. Phytane has a $\delta^{13}C$ value of −20‰. $\delta^{13}C$ values of steranes range from −21‰ to −13‰, whereas 17β(H),21β(H)-C_{34} hopane is strongly ^{13}C-depleted (−74‰).

5 Discussion

5.1 Modes of carbonate formation

Both macroscopic and petrographic observations allow to differentiate the studied sulfur-bearing carbonates into two categories: (1) macroscopically unaltered, where dolomite is the main sulfur-bearing carbonate phase (i.e., the laminated carbonate) and (2) diagenetically altered with calcite as sulfur-bearing carbonate phase (i.e., the brecciated carbonates). Microbial sulfate reduction driving the formation of authigenic carbonate and native sulfur may only occur after gypsum dissolution. However, the explanation of gypsum replacement in the laminated carbonate by dolomite and native sulfur is not straightforward since low-temperature formation of dolomite is kinetically inhibited. Microbial activity arguably mitigates these kinetic constraints, enabling dolomite formation at low temperature (for a review see Petrash et al., 2017 and references therein). Specifically, SRB are suspected to play a key role due to their ability to mitigate potential inhibiting and catalyzing factors (Lippmann, 1973; Kastner, 1984; Burns and Baker, 1987; Markham et al., 2002; Zhang et al., 2012; Lu et al., 2018) and being present at many sites of contemporary dolomite formation (Bontognali et al., 2012; 2014; Krause et al., 2012; Lu et al., 2021).

Abiotic dolomitization textures like neomorphic dolomite rhombs are lacking in both the laminated carbonate and the dolomite-rich clasts in the brecciated carbonate. Rather, peloidal and aphanitic microcrystalline fabrics are observed (Figures 2B,C), which are considered as evidence of a microbial contribution to carbonate precipitation (Flügel, 2004). Microbial mediation is further supported by $\delta^{13}C$ values of the laminated carbonate ($\delta^{13}C$ = −7.0‰ and −6.8‰) and the dolomite-rich clasts in the brecciated (1) carbonate sample ($\delta^{13}C$ = −10.3‰), revealing a contribution of organic carbon to carbonate formation. In addition, the formation of dolomite requires magnesium ions. Evaporation and gypsum precipitation likely concentrated magnesium in the brines (Rouchy et al., 1998), favoring dolomite formation (Warren, 2000). ^{18}O-enrichment of the dolomite-rich carbonate with $\delta^{18}O$ values as high as 2.6‰ and abundant gypsum pseudomorphs agree with evaporitic conditions during dolomite formation in the laminated and the dolomite-rich clasts in the brecciated carbonate. Positive $\delta^{18}O_{carbonate}$ values are generally explained by the evaporation of seawater, as ^{16}O partitions more easily into the water vapor phase and consequently the residual solution becomes enriched in ^{18}O (Ziegenbalg et al., 2010). The new Lorca oxygen isotope data is consistent with previous isotope data from primary evaporitic dolomites of the Lorca Basin (Rouchy et al., 1998).

The laminated carbonate and the dolomite-rich clasts in the brecciated carbonate formed similarly, as evidenced by petrography and stable isotope composition. However, post-depositional alteration caused the later formation of sulfur-bearing calcite in the brecciated carbonates, as demonstrated by its precipitation between the brecciated clasts (Figure 2B). The $\delta^{13}C$ value of sulfur-bearing calcite (as low as −18.9‰) in the brecciated carbonates also indicates a higher contribution of carbon derived from microbial oxidation of organic compounds (cf. Ziegenbalg et al., 2010; Caesar et al., 2019). Moreover, negative $\delta^{18}O$ values of calcite as low as −1.5‰ reflect precipitation from meteoric water (Ziegenbalg et al., 2010) rather than evaporation. Likewise, the sparitic matrix (i.e., the sulfur-bearing calcite) shows a tenfold decrease in CAS content compared to clasts (752 ppm and 7,121 ppm respectively), which is characteristic for meteoric diagenesis (Gill et al., 2008). Evidently, influx of meteoric water led to the dissolution of gypsum and possibly reduced the volume of the original dolomite-rich carbonate, causing brecciation. The change from hypersaline to meteoric conditions and the concomitant brecciation of the original rock implies that both the influx of meteoric water and the formation of sulfur-bearing calcite in case of the brecciated carbonates occurred significantly later after gypsum deposition and sedimentary lithification (i.e., during early diagenesis). A possible mechanism to explain this scenario is that the pre-evaporitic succession of the Lorca Basin was characterized by repeated opening and restriction (cf. Rouchy et al., 1998). The re-opening of the Lorca Basin could have potentially introduced "fresher" water into the subsurface, subsequently causing gypsum

dissolution, though this is a speculation as dating of the rocks is difficult.

Evidently, the two sulfur-bearing carbonates have different modes of formation. The formation of sulfur-bearing calcite in the brecciated carbonates was triggered by meteoric water influx significantly after sedimentary lithification, as evidenced by brecciation, and the peculiar oxygen isotope composition. Dolomite, calcite and native sulfur in the laminated carbonate precipitated during or shortly after gypsum deposition, as evidenced by the relatively undisturbed laminae, mineralogy, and the oxygen isotope composition. Because different pathways of formation are proposed, different modes of native sulfur genesis are probable. Both carbonate lithologies lack any petrographic evidence for native sulfur formation by bacterial sulfide oxidation (i.e., filamentous microfossils), as found in other sulfur-bearing carbonates of the Lorca Basin (Andreetto et al., 2019). In the brecciated carbonates, a possible mechanism for native sulfur formation could be meteoric water supplying molecular oxygen for abiotic sulfide oxidation. Native sulfur in the brecciated carbonates is less ^{34}S-enriched (13.1‰) than gypsum in the pre-evaporitic sediments ($\delta^{34}S_{mean}$ = 20.3‰ and 23.3‰, cf. Garcias Veigas et al., 2020; Playa et al., 2000). Furthermore, CAS reveals even more ^{34}S-enrichment during the precipitation of the sulfur-bearing calcite (54.3‰) compared to the dolomite clast (35.5‰). The ^{34}S-depletion of native sulfur with respect to gypsum and the range of ^{34}S-enrichment between sulfur and sulfate bearing phases ($\Delta^{34}S$ = 40.3‰) is akin to other sulfur deposits affected by meteoric diagenesis ($\Delta^{34}S$ = 41‰–66‰; Labrado et al., 2019). Differences in the S isotopic composition here between CAS, gypsum, and native sulfur mimic the isotope pattern reported for moderate to restricted fluid flow and limited to no supply of molecular oxygen in those deposits (cf. Labrado et al., 2019). These observations suggest that hydrogen sulfide oxidation was negligible or did not occur. Consequently native sulfur was most likely formed in an anoxic setting by a yet unknown mechanism (Labrado et al., 2019).

Evidence for gypsum dissolution by meteoric water is lacking for the laminated carbonate (positive $\delta^{18}O$ values; Table 1). The CAS content of the laminated carbonate is significantly lower (3,668 and 3,669 ppm) than in the dolomite-rich clasts of the brecciated (1) carbonate (7,121 ppm). Sulfate consumption by SRB lowers sulfate concentrations, causing sulfate undersaturation and subsequent gypsum dissolution, as reported for other gypsum deposits (Bąbel, 2007; De Lange and Krijgsman, 2010; Natalicchio et al., 2021). Prominent sulfate reduction was taking place in the depositional environment as evidenced by the presence of organic sulfur compounds (cf. Benali et al., 1995; Russell et al., 1997, Russell et al., 2000; Rouchy et al., 1998). Maximum ^{34}S-fractionation between CAS and native sulfur ($^{34}\Delta$ = 18.3‰) is also within the range reported for bacterial sulfate reduction in natural environments (Habicht and Canfield, 1997; Canfield, 2001; Detmers et al., 2001; Wortmann et al., 2001; Avrahamov et al., 2014). Assuming dolomite precipitation was mediated by SRB, lowered sulfate levels are further supported by the dolomite rims and dolomite pseudomorphs after gypsum (Figure 2A). With ongoing sulfate consumption and gypsum dissolution though, calcium ions were released and carbonate formation shifted from dolomite to calcite during later stages of carbonate formation, as evidenced by pseudomorphs after gypsum with calcite cores and dolomite rims (Figure 2A). Similar to calcite, native sulfur formation also occurred after gypsum dissolution, as evidenced by its occurrence as pseudomorphs after gypsum (Figure 2B). The ^{34}S-enrichment of native sulfur, nearly identical to pre-evaporitic gypsum, also supports complete consumption and no external supply of sulfate. Additionally, this suggests no external supply of molecular oxygen for sulfide oxidation either. Yet, this interpretation is solely based on isotope patterns reported for (semi-)closed systems of sulfur deposits formed significantly after sedimentary deposition (i.e., epigenetic formation; Labrado et al., 2019), whereas the depositional basin environment was not physically closed with regard to sulfur cycling. Native sulfur formation in the laminated carbonate likely formed by an unknown mechanism in an anoxic setting, though sulfide oxidation cannot be ruled out completely due to the architecture of the basin and its unknown physical processes of transporting molecular oxygen.

5.2 Disentangling molecular signals of the depositional environment

In Messinian replacement carbonates dominated by calcite, biomarkers of SRB were found to be akin to biomarkers found in methane-seep deposits (Ziegenbalg et al., 2012). In those calcium carbonates and at methane seeps, lipid biomarkers of SRB are easily discerned by their extreme ^{13}C-depletion, due to their syntrophic relation with ANMEs (Elvert et al., 2003; Blumenberg et al., 2004; Niemann and Elvert, 2008). In great contrast to these earlier observations, the laminated Lorca carbonate does not contain extremely ^{13}C-depleted archaeal and bacterial lipid biomarkers. The majority of microbially-derived compounds in the laminated carbonate shows $\delta^{13}C$ values ranging from roughly −25‰ to −15‰ (Figure 4). Therefore, it is rather challenging to distinguish biomarkers of SRB from other signals of the depositional environment. Petrography and isotope data suggest that the dolomite-rich clasts of the brecciated carbonates likely precipitated in a similar fashion as the laminated carbonate. In accord with those observations, the biomarker inventories of the laminated carbonate and brecciated carbonates include many similar compounds with similar ^{13}C-depletion, which supposedly derive from the sedimentary depositional environment of the Lorca Basin. The brecciated carbonates, however, have been altered post-depositional, changing its biomarker inventory and adding additional compounds lacking in the laminated carbonate.

A proxy for the sedimentary organic matter input is the presence of long-chain *n*-alkanes (C_{27-33}), which derive from leaf waxes of terrestrial plants (Eglinton and Eglinton, 2008). Both laminated and brecciated carbonates contain similar long-chain *n*-alkane patterns, although these compounds are more prominent in the laminated carbonate (Supplementary Table S1). Their $\delta^{13}C$ values are in the same range (−29‰ to −21‰) and reflect a mixture of C_3 plants (−38‰ to −32‰) and C_4 plants (−25‰ to −18‰; Collister et al., 1994; Naafs et al., 2012).

Organic sulfur compounds are present in both lithologies, although they are more abundant in the laminated carbonate. They form either through reactive organic compounds

incorporating sulfur (intramolecular), ending up as free organic sulfur compounds, or through sulfide bridges between individual compounds (intermolecular), ending up as sulfurized macromolecules (Werne et al., 2004; Amrani, 2014; Kutuzov et al., 2020). Organic sulfur compounds provide further insight into the original sedimentary input present during bacterial sulfate reduction, as reactive organic compounds are otherwise easily degraded. Sulfurization under euxinic conditions in the water column would probably have preserved compounds specific of anoxygenic phototrophic bacteria or organisms living in stratified water bodies, such as isorenieratane (Sinninghe Damsté et al., 1995; Wakeham et al., 2012; Sabino et al., 2021) and tetrahymanol or its degradation product gammacerane (Repeta et al., 1989; Van Gemerden and Mas, 1995; Wakeham et al., 2007; Sala et al., 2021), respectively. Both lipids were not observed in the bitumen and the desulfurized asphaltenes, arguing against water column euxinia and stratification at the time of deposition. The sulfurization of the lipids therefore rather took place in the sediment. Both types of sulfur-bearing carbonates exhibit similar inventories of organic sulfur compounds with similar $\delta^{13}C$ values from −23‰ to −12‰. Phototrophic microalgae were present during the sedimentary deposition of both carbonates as evidence by sulfurized C_{25} HBIs ($\delta^{13}C$ = −21‰ to −19‰), which derive from marine diatoms (Sinninghe Damsté and Rijppstra, 1993; 1999; Volkman et al., 1994; Grossi et al., 2004). Marine diatoms were continuously present in the basin leading to diatomite deposition during periods of high productivity in the pre-evaporitic period of the Lorca Basin (Rouchy et al., 1998). C_{25} HBIs are known to sulfurize fast and completely within ca. 500 years after deposition (Wakeham et al., 1995; Werne et al., 2000; Sinnighe Damsté et al., 2007).

The sulfurized HBIs are accompanied by various sulfurized steranes; sulfurization of steranes is supposed to be somewhat slower but is completed after 1,000–3,000 years after deposition (Kok et al., 2000). The source of steranes is ambiguous, possibly including algae and higher plants (Huang and Meinschein, 1979; Volkman, 1986). Steranes in the laminated and brecciated carbonates are dominated by C_{27} and C_{29} steranes. Similar sulfurized steranes are found in Lorca Basin shales (Benali et al., 1995). Sterane ratios can be used to identify their origin, but sulfurization preferentially affects C_{27} sterols and stanols over C_{29} sterols and stanols (Kok et al., 2000; Wang et al., 2004). The $\delta^{13}C$ values of C_{27} to C_{30} steranes from the desulfurized fraction are relatively uniform in both the laminated (−19‰ to −15‰) and the brecciated carbonates (from −21‰ to −13‰), suggesting similar sources. Moreover, the isotopic values are in the same range as those of HBIs and other organic sulfur compounds.

Both types of Lorca carbonates also contain free and sulfur-bond acyclic isoprenoids. One source of acyclic isoprenoids are archaeal cell membranes (Tornabene et al., 1979; Brassell et al., 1981; Chappe et al., 1982; Rowland, 1990; Grice et al., 1998), but some isoprenoids, like phytane and pristane, may also derive from the degradation of the phytol chain of chlorophyll (Powell and Mc Kirdy, 1973; Didyk et al., 1978). The free isoprenoids vary in their $\delta^{13}C$ values from −18‰ to −16‰ for the laminated carbonate, phytane in the brecciated carbonate shows a similar $\delta^{13}C$ value of −15‰. Such range partially overlaps with the $\delta^{13}C$ values of free phytane (−17‰ to −12‰) in the brecciated carbonate, and phytane released by desulfurization of the asphaltenes from both carbonates, ranging from −20‰ to −17‰. At first glance, such pattern seems to suggest a common source of free and sulfurized acyclic isoprenoids from the water column, as observed for the sulfurized steranes and the HBIs. However, an alternative, archaeal source for both compounds needs to be considered since high contents of archaeol are found in the laminated carbonate; archaeol is a common membrane lipid among archaea (Tornabene et al., 1979; Kates, 1993; Hinrichs et al., 1999; Dawson et al., 2012; Tourte et al., 2020). Archaeol may be degraded to phytane, yet free phytane in the brecciated carbonate (1) sample does not show similar $\delta^{13}C$ values as archaeol, disagreeing with archaeol as source compound. However, the isotopic fingerprint of archaeol-derived phytane after ether cleavage in the laminated carbonate is only slightly heavier (−19‰) than the free and sulfur-bound phytanes. Although the phytane isotope compositions after ether cleavage reflect a mixture of archaeol, phytanol, and extended archaeol, the major part is derived from archaeol, which is significantly more abundant than the other isoprenoids in the alcohol fraction. Since the isotopic signature of all phytanes are more or less similar and the isotopic signature of lipids from phototrophic algae are in the same range, phytane apparently represents a chlorophyll-derivative in this case, although minor contribution from archaea cannot be excluded.

At least two archaeal communities were likely present in the depositional environments of the laminated carbonate and the dolomite-rich clasts in the brecciated carbonate. Extended archaeol, a biomarker of halophilic archaea (Teixidor et al., 1993; Dawson et al., 2012), was found in both the laminated and the brecciated carbonates. It is used as a salinity proxy as it is not produced below 50 psu (Vandier et al., 2021). Regular PMI, which was identified after ether cleavage of extended archaeol, shows a similar ^{13}C-depletion as extended archaeol found in Messinian filament-bearing gypsum (Natalicchio et al., 2022). More evidence for the presence of archaea in the depositional environments stems from minor amounts of acyclic biphytane observed after ether cleavage of GDGT-0, a transmembrane lipid produced by several archaeal families but not by Haloarchaea (Bauersachs et al., 2015; Bale et al., 2019; Tourte et al., 2020). Beside archaeal lipids, bacterial non-isoprenoid McDGs are present in the laminated and brecciated carbonates, further supporting the scenario of enhanced salinity during sedimentary carbonate formation. Initially reported by Baudrand et al. (2010) as products of extremophilic bacteria, McDGs have since then been reported for a wide variety of environments with either increased salinity or gypsum dissolution (Ziegenbalg et al., 2012; Aloisi et al., 2013; Birgel et al., 2014; Sorokin et al., 2021; Natalicchio et al., 2022).

The involvement of sulfide-oxidizing bacteria in native sulfur formation, as suggested by Andreetto et al. (2019), cannot be confirmed by lipid biomarkers. Major lipids of sulfide-oxidizing bacteria are saturated and unsaturated C_{16} and C_{18} fatty acids (McCaffrey et al., 1989; Zhang et al., 2005; Arning et al., 2008). Saturated C_{16} and C_{18} fatty acids are abundant in the laminated carbonate and show similar $\delta^{13}C$ values as other lipids, but such compounds can be produced by a wide variety of organisms and are therefore not diagnostic. Unsaturated C_{18} fatty acids were also likely present during bacterial sulfate reduction as evidenced by thiophenic C_{18} fatty acids in the laminated carbonate. To conclude, these biomarkers are not source-specific as they are produced by a large variety of microorganisms including SRB

(Stackebrandt, 2014). Since sulfide-oxidizing bacteria cannot be traced by lipid biomarkers, their involvement in native sulfur formation cannot be excluded.

5.3 Biomarker evidence of bacterial sulfate reduction and its role in native sulfur formation in the laminated carbonate

Assignment of biomarkers in the laminated carbonate to SRB is difficult because $\delta^{13}C$ values do not allow discerning such biomarkers confidently from those of other microbial groups. Other evidence for microbial sulfate reduction is the large isotopic fractionation between CAS and native sulfur, the presence of organic sulfur compounds and, to a lesser extent, the $\delta^{13}C_{carbonate}$ values of both clay- and dolomite-rich laminae and the presence of dolomite. The mid-chain branched fatty acid 10Me-C_{16} is commonly assigned to SRB (Taylor and Parkes, 1983; Elvert et al., 2003; Londry et al., 2004; Vinçon-Laugier et al., 2017), yet it is only present in small amounts compared to the other biomarkers in the laminated carbonate. Terminally branched fatty acids are also common in marine SRB (Kaneda, 1991). *Iso*- and *anteiso*-C_{15} and -C_{17} fatty acids, with a predominance of *iso* over *anteiso*, and *iso*-C_{16} fatty acids are synthesized by a wide variety of SRB (Stackebrandt, 2014; Zakharyuk et al., 2015; Thioye et al., 2017; Watanabe et al., 2017; Spring et al., 2019). Other fatty acids common in SRB are saturated C_{14} to C_{18} fatty acids, and unsaturated C_{16} and C_{18} fatty acids.

The $\delta^{13}C$ values of *iso*-C_{15}, *iso*-C_{16}, and *iso*-C_{17} fatty acids (−19‰, −18‰, −17‰, respectively) agree with a common source, likely representing SRB. The $\delta^{13}C$ values of saturated C_{14} to C_{18} fatty acids are lower (−25‰ to −23‰), possibly indicating multiple producers including SRB. The *iso*-C_{15}, *iso*-C_{16}, and *iso*-C_{17} fatty acids assigned to SRB reveal $\delta^{13}C$ values indistinguishable from other compounds from the depositional environment, agreeing with organoclastic sulfate reduction. Minor ^{13}C-fractionation in the lipids of SRB compared with substrates has been observed in culture experiments (Londry and des Marais, 2003; Londry et al., 2004) and reef microbialites (Heindel et al., 2010; 2012). During culture studies, little fractionation was found to be associated with heterotrophic growth (i.e., organoclastic sulfate reduction), consistent with observations made for heterotrophic microorganisms in general (Hayes, 1993; Abraham et al., 1998). Culture studies also showed that fatty acids produced by *Desulfotomaculum acetoxidans* have relatively high $\delta^{13}C$ values when substrate is limited. Other species of SRB grown under similar conditions did not reproduce these results, and it has been suggested that high $\delta^{13}C$ values can be used as an indication for growth substrate availability when *Desulfotomaculum* species are dominant (Londry et al., 2004). Coincidentally, *iso*-C_{15} and *iso*-C_{17} fatty acids are produced in significant amounts by *Desulfotomaculum* species (Parshina et al., 2005; Stackebrandt, 2014). Still, caution is required when using such information for the reconstruction of paleoenvironments, since carbon isotope fractionation in bacteria is affected by complex processes such as enzymatic pathways, microbial interactions and environmental conditions (Londry and des Marais, 2003). Heindel et al. (2012) suggested a combination of enzymatic ^{13}C-enrichment and bacterial consumption of isotopically heavy extracellular polymeric substances (EPS) to explain relatively ^{13}C-enriched lipids of SRB in reef environments. Microbes secrete EPS, which mainly consists of polysaccharides (Decho, 1990; Sutherland, 2001).

The obtained sulfur isotope data seem to suggest that molecular oxygen was low to absent during native sulfur formation in the laminated carbonate (see above), rendering abiotic or bacterial sulfide oxidation unlikely. Interestingly, SRB have recently been reported to form native sulfur (Zhang et al., 2020; Cai et al., 2022; Liu et al., 2022). SRB responding to salt stress is another potential mechanism for native sulfur formation (cf. Labrado et al., 2019). Marine sediments in the Lorca Basin have a high dolomite content but, contrary to the laminated carbonate, no native sulfur (Rouchy et al., 1998). The main differences between these Lorca Basin lithologies were probably different degrees of salinity as evidenced by gypsum pseudomorphs and the biomarkers of halophiles in the laminated carbonate. Under hypersaline conditions, microbes are required to cope with osmotic stress (e.g., Fernandes et al., 1993). This can suppress some metabolic processes, particularly processes yielding little energy (Brown, 1978; Welsh et al., 1996; Oren, 1999; Oren, 2013). Under stressed conditions, intermediate sulfur compounds used in microbial sulfate reduction can leak out of cells and can potentially form native sulfur (Fitz and Cypionka, 1990; Bishop et al., 2013). Such a scenario is supported by the presence of the non-isoprenoidal McDGs, membrane lipids that are arguably used to adapt to extreme, possibly sulfidic conditions. Other evidence is the relatively high $\delta^{13}C$ values of *iso*-C_{15}, *iso*-C_{16} and *iso*-C_{17} fatty acids that suggest substrate limitation or consumption of isotopically heavy substrate (see above).

5.4 Biomarker evidence of methanogenesis, AOM, and bacterial sulfate reduction in the brecciated carbonates

The brecciated carbonates contain extremely ^{13}C-depleted lipids similar to biomarkers of SRB and ANME found at marine methane seeps (Peckmann and Thiel, 2004; Birgel et al., 2008; Niemann and Elvert, 2008; Ziegenbalg et al., 2012; Thiel, 2020). Yet, different degrees of ^{13}C-depletion are observed among these biomarkers. The strong, uniform ^{13}C-depletion of macrocyclic archaeol, acyclic biphytanic diacid (bp-0), and *sn2*-hydroxyarchaeol ($\delta^{13}C$ = −65‰, −64‰, −62‰, respectively) suggests a common archaeal source. Whereas *sn2*-hydroxyarchaeol is common in various methanogens and methanotrophs (Koga et al., 1998; Peckmann and Thiel, 2004), macrocyclic archaeol is more specific for thermophilic autotrophic methanogens (Comita et al., 1984; Baumann et al., 2018). Acyclic biphytanic diacid is a degradation product of GDGT-0 (Liu et al., 2016), which is occasionally found in sediments and more commonly in carbonates (Schouten et al., 2003; Birgel et al., 2008; Smrzka et al., 2017). Taken together, these lipids mimic the order-specific membrane composition of the haloalkaliphilic methanogen *Methanosalsum natronophilum* (Bale et al., 2019). Thus, it is likely that these archaeal lipids are indeed derived from methanogens similar to *M. natronophilum*. *Methanosalsum natronophilum* also produces GDGT-0 as major membrane lipid, like other methanogens (Koga et al., 1998; Bauersachs et al., 2015). Abundant acyclic biphytane after ether cleavage is indeed present in the Lorca brecciated carbonate,

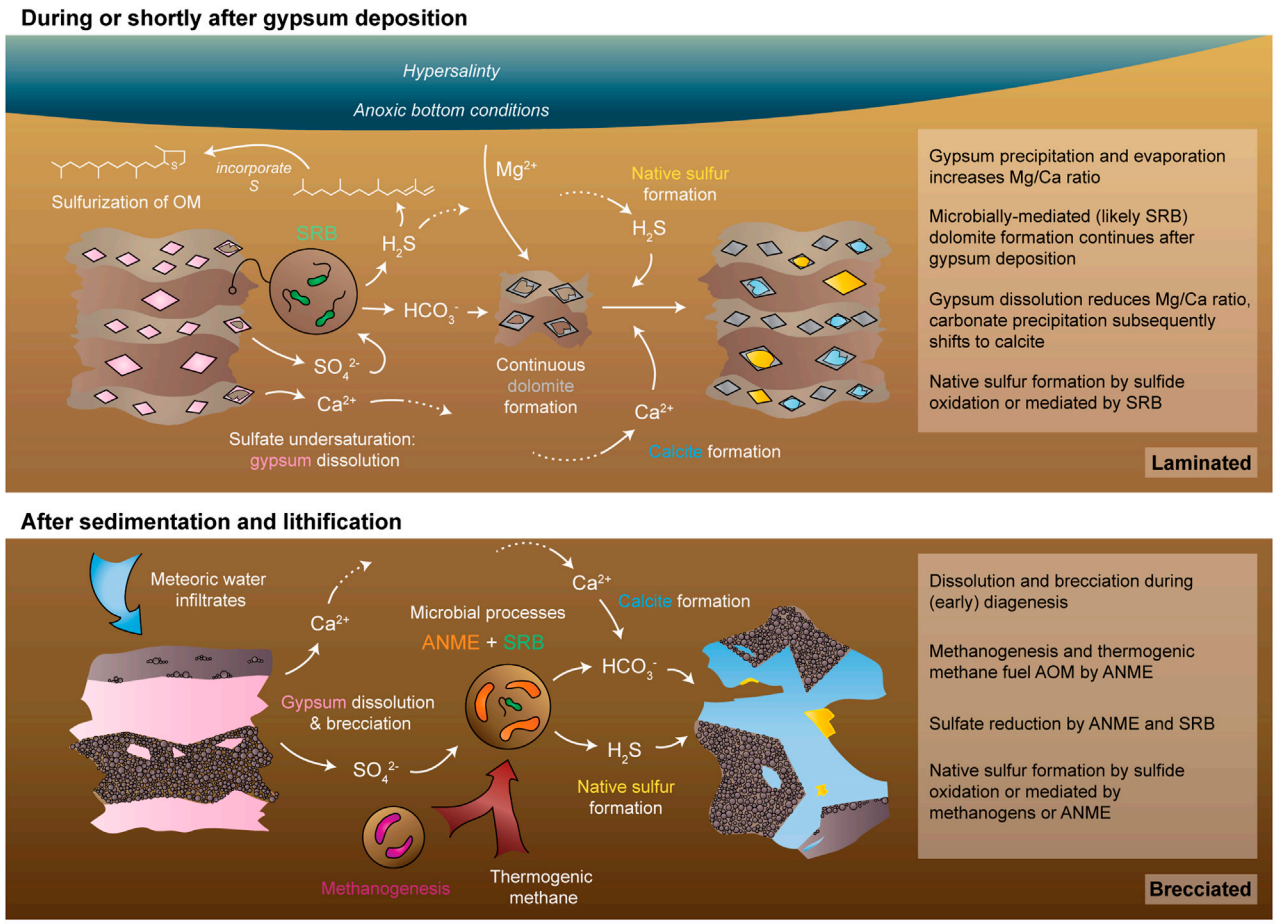

FIGURE 5
Sketch showing the sequential formation of laminated and brecciated sulfur-bearing carbonates (from left to right) and the relative time relations of different paragenetic events in respect to the original deposition of gypsum. Circles indicate microbial communities (orange = anaerobic methanotrophic archaea = ANME, green = sulfate-reducing bacteria, purple = methanogens).

but with a lower $\delta^{13}C$ value of −81‰. Moreover, acyclic biphytane is accompanied by ^{13}C-depleted mono- and bicyclic biphytanes (−85‰ on average). Therefore, acyclic biphytane is possibly deriving from mixed archaeal sources. One source is probably methanogens related to *M. natronophilum*, producing both GDGT-0 and macrocyclic archaeol.

Source organisms of the ring-containing GDGTs present in the brecciated Lorca carbonate probably did not include methanogens, since methanogens have rarely been described to produce these membrane lipids (Bauersachs et al., 2015). The corresponding ^{13}C-depleted biphytanes may rather derive from methanotrophic archaea since ANMEs produce such GDGT patterns (Blumenberg et al., 2004). Similarly, PMI is characteristic for ANMEs (Elvert et al., 1999; Thiel et al., 1999; Ziegenbalg et al., 2012), but also for some methanogens (e.g., Brassell et al., 1981; Schouten et al., 1997; Londry et al., 2008). Its ^{13}C-depletion (−88‰), however, implies that AOM was involved in (secondary) carbonate authigenesis of the brecciated carbonates. At methane seeps dominated by an ANME-2 community, ^{13}C-depleted PMI is typically found together with

^{13}C-depleted crocetane (Peckmann and Thiel, 2004; Niemann and Elvert, 2008; Thiel, 2020), yet crocetane is missing in the brecciated carbonates. The lack of crocetane mimics the biomarker pattern of Sicilian sulfur-bearing carbonates described by Ziegenbalg et al. (2012) and suggests the presence of ANME-1 like communities during secondary (calcium) carbonate precipitation. Such communities are also known to produce ring-containing GDGTs, contrary to other ANME communities (Blumenberg et al., 2004; Rossel et al., 2008; 2011; Bertram et al., 2013). Although this could mean that similar ANME communities were involved in the sulfur-bearing calcite formation of the brecciated Lorca carbonates, Ziegenbalg et al. (2012) also found ^{13}C-depleted *sn3*-hydroxyarchaeol in the Sicilian carbonates, a compound not observed in the brecciated Lorca carbonates.

Characteristic biomarkers of methanogens were not found in the Sicilian sulfur-bearing carbonates (Ziegenbalg et al., 2012). However, both sulfur cycling and methanogenesis are observed in the hypersaline and sulfidic environment of the Urania deep basin (Borin et al., 2009). Labrado et al. (2019) calculated that under such hypersaline conditions, sulfide oxidation coupled to methanogenesis using methylated substrates ('methylotrophic') is a thermodynamically viable mechanism for native sulfur formation. In accordance with such results, methylotrophic methanogenesis is the dominant methanogenic pathway in hypersaline environments and methylated substrates are commonly widely available under such conditions (Zhuang et al., 2016; McGenity and Sorokin, 2018). Interestingly, the halotolerant *M. natronophilum* was also cultured on methanol (Bale et al., 2019). Thus, the biomarker evidence reported herein supports sulfide oxidation coupled to methylotrophic methanogenesis.

For some settings, methanogenesis has been reported to fuel AOM in a so-called "cryptic methane cycle" (Xiao et al., 2017; 2018). Biogenic methane has a δ^{13}C value ranging from −110‰ to −50‰, whereas thermogenic methane is ranging from −50‰ to −20‰ (Whiticar, 1999). Interestingly, ^{13}C-fractionation between the oxidized methane and PMI produced by ANMEs typically ranges from −60‰ to −20‰ (Miyajima et al., 2020). Therefore, the δ^{13}C value of methane in the Lorca Basin would have been in the range from −68‰ to −28‰. This suggests that AOM was fueled by thermogenic methane or a mixture of thermogenic and biogenic methane. Alternatively, substrate limitation during (methylotrophic) methanogenesis could result in isotopically heavy methane. Experiments with the methanogen *Methanosarcina barkeri* showed ^{13}C-enrichment for methane in the experiment's headspace (Londry et al., 2008). The overall inventory of archaeal lipids including ^{13}C-depleted archaeol and squalane agree with the presence of different archaeal communities during carbonate formation (e.g., Tornabene et al., 1979; Grice et al., 1998) such as halophiles (extended archaeol δ^{13}C = −12‰), methanogens, and ANMEs.

ANME at marine seeps typically form syntrophic partnerships with SRB (Boetius et al., 2000; Orphan et al., 2001; Nauhaus et al., 2005; Niemann and Elvert, 2008). Characteristic SRB biomarkers, such as terminally branched fatty acids, indeed occur in the brecciated carbonates. However, these SRB biomarkers do not show the strong ^{13}C-depletion that is typical of seep-dwelling SRB. Rather, the observed terminally branched fatty acids show ^{13}C-depletion similar to biomarkers of the sedimentary environment (e.g., organic sulfur compounds). In the Sicilian sulfur-bearing carbonates, terminally branched fatty acids were found to be strongly ^{13}C-depleted (Ziegenbalg et al., 2012). Evidence for SRB involved in AOM only comes from strongly ^{13}C-depleted 17β(H),21β(H)-C_{34} hopane (δ^{13}C = −74‰) in the desulfurized fraction of the brecciated Lorca carbonates. This hopane likely derived from a sulfurized bacteriohopanepolyol (cf. Xavier et al., 1997; Blumenberg et al., 2010). Strongly ^{13}C-depleted hopanoids found together with markers of ANME have been interpreted to derive from SRB (Pancost et al., 2000; Thiel et al., 2003; Blumenberg et al., 2006). Another biomarker for SRB in the brecciated carbonate is a non-isoprenoidal C_{36} DAGE. DAGEs found at seeps are also associated with the syntrophic AOM communities (e.g., Hinrichs et al., 2000; Aloisi et al., 2002; Teske et al., 2002; Chevalier et al., 2010). After ether cleavage, 10Me-C_{16} alkane and C_{16} alkane (δ^{13}C = −76‰, −67‰, respectively) were found. The 10Me-C_{16} alkane therefore reveals a similar depletion as the hopanoid. The C_{16} alkane is slightly less depleted, most likely due to an additional contribution from a C_{16} alcohol after ether cleavage. We therefore assume that the C_{36} DAGE is composed of a 10Me-C_{16} and *n*-C_{16} hydrocarbon chain. The same compound has been reported for mesophilic SRB (Grossi et al., 2015; Vinçon-Laugier et al., 2016). In the brecciated carbonate, SRB lipids are roughly 10‰ less ^{13}C-depleted than the ANME lipids, which is consistent with the isotopic offset observed at methane seeps (Orphan et al., 2002), where the DAGE-producing SRB are possibly heterotrophs and may be using various substrates although they are closely associated with AOM (Krake et al., 2022). However, in the present case, the lack of the characteristic ^{13}C-depleted biomarkers and the small amounts of hopane and C_{36} DAGE (see Supplementary Table S1) suggest that the contribution of SRB to the formation of the secondary carbonate was small, possibly even negligible.

Instead, sulfate reduction may have been conducted by ANME alone (Milucka et al., 2012; Antler et al., 2014). Coincidentally, such methanotrophic sulfate reduction resulting in calcite precipitation after gypsum dissolution is another possible mechanism for native sulfur formation that is thermodynamically viable (cf. Labrado et al., 2019). Further evidence for such a mechanism is that sulfur formation was observed within the cells of ANME (Milucka et al., 2012). Noteworthy, ANME-1 are more loosely associated with SRB (Bertram et al., 2013; Gründger et al., 2019) and are reported to be involved in a 'cryptic methane cycle' (Beulig et al., 2019; Kevorkian et al., 2021). Although all this is circumstantial evidence, together with the biomarker data (e.g., lack of crocetane, prominent GDGTs), an ANME-1-like community appears the most probable candidate involved in the sulfur-bearing calcite formation of the brecciated carbonates.

6 Conclusion

Two types of sulfur-bearing carbonates from the Lorca Basin studied herein suggest different modes of formation (Figure 5). A sulfur-bearing, laminated carbonate, consisting of clay-rich and dolomite-rich laminae, precipitated during gypsum deposition in a hypersaline, restricted basin environment. Dolomite formation was microbially mediated, likely by sulfate-reducing bacteria (SRB). Subsequent sulfate undersaturation caused gypsum dissolution, releasing sulfate for continuous sulfate reduction and dolomite formation. Either during or shortly after gypsum

deposition, pseudomorphs of dolomite after gypsum formed. Simultaneously, the sulfurization of organic matter was favored by the production of hydrogen sulfide by SRB. With ongoing gypsum dissolution and the release of calcium ions, calcite nuclei in gypsum pseudomorphs show that carbonate formation shifted to calcite during later stages of carbonate formation. Native sulfur formation in the laminated carbonate was synchronous with dolomite and calcite formation as gypsum pseudomorphs. Native sulfur formation was likely mediated by SRB, possibly representing a stress response to high salt concentrations, although sulfide oxidation cannot be ruled out. The laminated carbonate is most likely recording (local) environmental change shortly after deposition.

In case of the brecciated carbonates, the formation of sulfur-bearing carbonate is the result of a later-stage diagenetic formation process. The dolomite-rich clasts in the brecciated carbonate rock reflect initial carbonate deposition in a restricted basin environment, similar to the laminated carbonate. Meteoric water dissolved gypsum significantly after sedimentation and lithification, causing the brecciation of the original, sedimentary carbonate. During the subsequent precipitation of sulfur-bearing calcite, the environment was shaped by methanogens, anaerobic methane oxidizing archaea (ANME) and SRB. Native sulfur formation was the consequence of microbial metabolisms. Such mediation was either methanogens oxidizing hydrogen sulfide likely under hypersaline conditions or methanotrophic sulfate reduction coupled to gypsum dissolution and calcite formation. Previously unreported, the brecciated carbonate contains evidence of the activity of methanogens during the formation of a gypsum-replacing carbonate. For both studied types of sulfur-bearing carbonates evidence is found that anaerobic bacteria and archaea might mediate native sulfur formation.

Data availability statement

The original contributions presented in the study are included in the article/Supplementary Material, further inquiries can be directed to the corresponding author.

Author contributions

SR, LG, GA, and J-MR collected samples in Spain. SR, DB, VG, and GA performed sample preparation, biomarker extraction, and biomarker analysis. SR and GA performed XRD analysis. LG performed native sulfur isotope analysis. ALL performed CAS content and sulfur isotope analysis. SR wrote the manuscript. DB and JP supervised the research and contributed to the writing. LG, VG, and GA contributed to the discussion. All authors revised the work critically and approved the manuscript. All authors listed have made a substantial, direct, and intellectual contribution to the work and approved it for publication. All authors contributed to the article and approved the submitted version.

Funding

This research was supported by the project SALTGIANT-Understanding the Mediterranean Salt Giant, a European project which has received funding from the European Union's Horizon 2020 research and innovation program, under the Marie Skłodowska-Curie [Grant Agreement No 765256].

Acknowledgments

We thank Eva Vinx for the preparation of thin sections, Henning Kühnert for carbon and oxygen stable isotope analysis of carbonate samples, Carsten Paulmann for assistance with XRD analysis, Sabine Beckmann for help with biomarker extraction and analysis, and the three reviewers for constructive comments that helped to improve the manuscript. Matthias Reimann and KNAUF Gips are acknowledged for their contribution to the SALTGIANT consortium.

Conflict of interest

The authors declare that the research was conducted in the absence of any commercial or financial relationships that could be construed as a potential conflict of interest.

The reviewer EL declared a past co-authorship with the author VG to the handling editor.

Publisher's note

Supplementary material

The Supplementary Material for this article can be found online at: https://www.frontiersin.org/articles/10.3389/feart.2023.1153415/full#supplementary-material

References

Abraham, W. R., Hesse, C., and Pelz, O. (1998). Ratios of carbon isotopes in microbial lipids as an indicator of substrate usage. *Appl. Environ. Microbiol.* 64 (11), 4202–4209. doi:10.1128/AEM.64.11.4202-4209.1998

Adam, P., Schmid, J. C., Albercht, P., and Connan, J. (1991). 2α and 3β Steroid thioIs from reductive cleavage of macromolecular petroleum fraction. *Tetrahedron Lett.* 32 (25), 2955–2958. doi:10.1016/0040-4039(91)80661-O

Aloisi, G., Baudrand, M., Lécuyer, C., Rouchy, J. M., Pancost, R. D., Aref, M. A. M., et al. (2013). Biomarker and isotope evidence for microbially-mediated carbonate formation from gypsum and petroleum hydrocarbons. *Chem. Geol.* 347, 199–207. doi:10.1016/j.chemgeo.2013.03.007

Aloisi, G., Bouloubassi, I., Heijs, S. K., Pancost, R. D., Pierre, C., Sinninghe Damsté, J. S., et al. (2002). CH_4-consuming microorganisms and the formation of

carbonate crusts at cold seeps. *Earth Planet. Sci. Lett.* 203 (1), 195–203. doi:10.1016/S0012-821X(02)00878-6

Amend, J. P., Aronson, H. S., Macalady, J., and LaRowe, D. E. (2020). Another chemolithotrophic metabolism missing in nature: Sulfur comproportionation. *Environ. Microbiol.* 22 (6), 1971–1976. doi:10.1111/1462-2920.14982

Amrani, A. (2014). Organosulfur compounds: Molecular and isotopic evolution from biota to oil and gas. *Annu. Rev. Earth Planet. Sci.* 42 (1), 733–768. doi:10.1146/annurev-earth-050212-124126

Anadón, P., Rosell, L., and Talbot, M. R. (1992). Carbonate replacement of lacustrine gypsum deposits in two Neogene continental basins, eastern Spain. *Sediment. Geol.* 78 (3-4), 201–216. doi:10.1016/0037-0738(92)90020-R

Andreetto, F., Aloisi, G., Raad, F., Heida, H., Flecker, R., Agiadi, K., et al. (2021). Freshening of the mediterranean salt giant: Controversies and certainties around the terminal (upper gypsum and lago-mare) phases of the Messinian salinity crisis. *Earth-Science Rev.* 216, 103577. doi:10.1016/j.earscirev.2021.103577

Andreetto, F., Dela Pierre, F., Gibert, L., Natalicchio, M., and Ferrando, S. (2019). Potential fossilized sulfide-oxidizing bacteria in the upper Miocene sulfur-bearing limestones from the Lorca Basin (SE Spain): Paleoenvironmental implications. *Front. Microbiol.* 10, 1031. doi:10.3389/fmicb.2019.01031

Antler, G., Turchyn, A. V., Herut, B., Davies, A., Rennie, V. C., and Sivan, O. (2014). Sulfur and oxygen isotope tracing of sulfate driven anaerobic methane oxidation in estuarine sediments. *Estuar. Coast. Shelf Sci.* 142, 4–11. doi:10.1016/j.ecss.2014.03.001

Arning, E. T., Birgel, D., Schulz-Vogt, H. N., Holmkvist, L., Jørgensen, B. B., Larson, A., et al. (2008). Lipid biomarker patterns of phosphogenic sediments from upwelling regions. *Geomicrobiol. J.* 25 (2), 69–82. doi:10.1080/01490450801934854

Avrahamov, N., Antler, G., Yechieli, Y., Gavrieli, I., Joye, S. B., Saxton, M., et al. (2014). Anaerobic oxidation of methane by sulfate in hypersaline groundwater of the Dead Sea aquifer. *Geobiology* 12 (6), 511–528. doi:10.1111/gbi.12095

Bąbel, M. (2007). Depositional environments of a salina-type evaporite basin recorded in the Badenian gypsum facies in the northern Carpathian Foredeep. *Geol. Soc. Lond. Spec. Publ.* 285, 107–142. doi:10.1144/SP285.7

Bale, N. J., Sorokin, D. Y., Hopmans, E. C., Koenen, M., Rijpstra, W. I. C., Villanueva, L., et al. (2019). New insights into the polar lipid composition of extremely halo(alkali) philic euryarchaea from hypersaline lakes. *Front. Microbiol.* 10, 377. doi:10.3389/fmicb.2019.00377

Baudrand, M., Aloisi, G., Lécuyer, C., Martineau, F., Fourel, F., Escarguel, G., et al. (2012). Semi-automatic determination of the carbon and oxygen stable isotope compositions of calcite and dolomite in natural mixtures. *Appl. Geochem.* 27 (1), 257–265. doi:10.1016/j.apgeochem.2011.11.003

Baudrand, M., Grossi, V., Pancost, R., and Aloisi, G. (2010). Non-isoprenoid macrocyclic glycerol diethers associated with authigenic carbonates. *Org. Geochem.* 41 (12), 1341–1344. doi:10.1016/j.orggeochem.2010.09.002

Bauersachs, T., Weidenbach, K., Schmitz, R. A., and Schwark, L. (2015). Distribution of glycerol ether lipids in halophilic, methanogenic and hyperthermophilic archaea. *Org. Geochem.* 83, 101–108. doi:10.1016/j.orggeochem.2015.03.009

Baumann, L. M., Taubner, R. S., Bauersachs, T., Steiner, M., Schleper, C., Peckmann, J., et al. (2018). Intact polar lipid and core lipid inventory of the hydrothermal vent methanogens *Methanocaldococcus villosus* and *Methanothermococcus okinawensis*. *Org. Geochem.* 126, 33–42. doi:10.1016/j.orggeochem.2018.10.006

Behrens, A., Schaeffer, P., and Albrecht, P. (1997). 14β, 22R-epithiosteranes, a novel series of fossil steroids widespread in sediments. *Tetrahedron Lett.* 38 (27), 4921–4924. doi:10.1016/S0040-4039(97)01059-9

Benali, S., Schreiber, B. C., Helman, M. L., and Philp, R. P. (1995). Characterization of organic matter from a restricted/evaporative sedimentary environment: Late Miocene of Lorca Basin, southeastern Spain. *AAPG Bull.* 79 (6), 816–829. doi:10.1306/8D2B1BBA-171E-11D7-8645000102C1865D

Bertram, S., Blumenberg, M., Michaelis, W., Siegert, M., Krüger, M., and Seifert, R. (2013). Methanogenic capabilities of ANME-archaea deduced from ^{13}C-labelling approaches. *Environ. Microbiol.* 15 (8), 2384–2393. doi:10.1111/1462-2920.12112

Beulig, F., Røy, H., McGlynn, S. E., and Jørgensen, B. B. (2019). Cryptic CH_4 cycling in the sulfate–methane transition of marine sediments apparently mediated by ANME-1 archaea. *ISME J.* 13 (2), 250–262. doi:10.1038/s41396-018-0273-z

Birgel, D., Elvert, M., Han, X., and Peckmann, J. (2008). ^{13}C-depleted biphytanic diacids as tracers of past anaerobic oxidation of methane. *Org. Geochem.* 39 (1), 152–156. doi:10.1016/j.orggeochem.2007.08.013

Birgel, D., Guido, A., Liu, X., Hinrichs, K.-U., Gier, S., and Peckmann, J. (2014). Hypersaline conditions during deposition of the Calcare di Base revealed from archaeal di- and tetraether inventories. *Org. Geochem.* 77, 11–21. doi:10.1016/j.orggeochem.2014.09.002

Birgel, D., Thiel, V., Hinrichs, K.-U., Elvert, M., Campbell, K. A., Reitner, J., et al. (2006). Lipid biomarker patterns of methane-seep microbialites from the Mesozoic convergent margin of California. *Org. Geochem.* 37 (10), 1289–1302. doi:10.1016/j.orggeochem.2006.02.004

Bishop, T., Turchyn, A. V., and Sivan, O. (2013). Fire and brimstone: The microbially mediated formation of elemental sulfur nodules from an isotope and major element study in the paleo-dead sea. *PLoS One* 8 (10), e75883. doi:10.1371/journal.pone.0075883

Blumenberg, M., Krüger, M., Nauhaus, K., Talbot, H. M., Oppermann, B. I., Seifert, R., et al. (2006). Biosynthesis of hopanoids by sulfate-reducing bacteria (genus *Desulfovibrio*). *Environ. Microbiol.* 8 (7), 1220–1227. doi:10.1111/j.1462-2920.2006.01014.x

Blumenberg, M., Mollenhauer, G., Zabel, M., Reimer, A., and Thiel, V. (2010). Decoupling of bio- and geohopanoids in sediments of the Benguela upwelling system (BUS). *Org. Geochem.* 41 (10), 1119–1129. doi:10.1016/j.orggeochem.2010.06.005

Blumenberg, M., Seifert, R., Reitner, J., Pape, T., and Michaelis, W. (2004). Membrane lipid patterns typify distinct anaerobic methanotrophic consortia. *Proc. Natl. Acad. Sci.* 101 (30), 11111–11116. doi:10.1073/pnas.0401188101

Boetius, A., Ravenschlag, K., Schubert, C. J., Rickert, D., Widdel, F., Gieseke, A., et al. (2000). A marine microbial consortium apparently mediating anaerobic oxidation of methane. *Nature* 407 (6804), 623–626. doi:10.1038/35036572

Bontognali, T. R., McKenzie, J. A., Warthmann, R. J., and Vasconcelos, C. (2014). Microbially influenced formation of Mg-calcite and Ca-dolomite in the presence of exopolymeric substances produced by sulphate-reducing bacteria. *Terra Nova.* 26 (1), 72–77. doi:10.1111/ter.12072

Bontognali, T. R., Vasconcelos, C., Warthmann, R. J., Lundberg, R., and McKenzie, J. A. (2012). Dolomite-mediating bacterium isolated from the sabkha of Abu Dhabi (UAE). *Terra nova.* 24 (3), 248–254. doi:10.1111/j.1365-3121.2012.01065.x

Borin, S., Brusetti, L., Mapelli, F., d'Auria, G., Brusa, T., Marzorati, M., et al. (2009). Sulfur cycling and methanogenesis primarily drive microbial colonization of the highly sulfidic Urania deep hypersaline basin. *Proc. Natl. Acad. Sci.* 106 (23), 9151–9156. doi:10.1073/pnas.0811984106

Brand, W. A., Coplen, T. B., Vogl, J., Rosner, M., and Prohaska, T. (2014). Assessment of international reference materials for isotope-ratio analysis (IUPAC Technical Report). *Pure Appl. Chem.* 86 (3), 425–467. doi:10.1515/pac-2013-1023

Brassell, S. C., Wardroper, A. M. K., Thomson, I. D., Maxwell, J. R., and Eglinton, G. (1981). Specific acyclic isoprenoids as biological markers of methanogenic bacteria in marine sediments. *Nature* 290 (5808), 693–696. doi:10.1038/290693a0

Brown, A. D. (1978). Compatible solutes and extreme water stress in eukaryotic micro-organisms. *Adv. Microb. Physiology* 17, 181–242. doi:10.1016/S0065-2911(08)60058-2

Brunner, B., and Bernasconi, S. M. (2005). A revised isotope fractionation model for dissimilatory sulfate reduction in sulfate reducing bacteria. *Geochimica Cosmochimica Acta* 69 (20), 4759–4771. doi:10.1016/j.gca.2005.04.015

Burns, S. J., and Baker, P. A. (1987). A geochemical study of dolomite in the Monterey Formation, California. *J. Sediment. Res.* 57 (1), 128–139. doi:10.1306/212F8AC6-2B24-11D7-8648000102C1865D

Caesar, K. H., Kyle, J. R., Lyons, T. W., Tripati, A., and Loyd, S. J. (2019). Carbonate formation in salt dome cap rocks by microbial anaerobic oxidation of methane. *Nat. Commun.* 10 (1), 808–809. doi:10.1038/s41467-019-08687-z

Cai, R., He, W., Liu, R., Zhang, J., Zhang, X., and Sun, C. (2022). Deep-sea *in situ* insights into the formation of zero-valent sulfur driven by a bacterial thiosulfate oxidation pathway. *mBio* 13 (4), e0014322–22. doi:10.1128/mbio.00143-22

Canfield, D. E. (2001). Isotope fractionation by natural populations of sulfate-reducing bacteria. *Geochimica Cosmochimica Acta* 65 (7), 1117–1124. doi:10.1016/S0016-7037(00)00584-6

Carpentier, C., Vennin, E., Rouchy, J. M., Cornée, J. J., Melinte-Dobrinescu, M., Hibsch, C., et al. (2020). Ages and stratigraphical architecture of late Miocene deposits in the Lorca Basin (Betics, SE Spain): New insights for the salinity crisis in marginal basins. *Sediment. Geol.* 405, 105700. doi:10.1016/j.sedgeo.2020.105700

Chappe, B., Albrecht, P., and Michaelis, W. (1982). Polar lipids of archaebacteria in sediments and petroleums. *Science* 217 (4554), 65–66. doi:10.1126/science.217.4554.65

Chevalier, N., Bouloubassi, I., Stadnitskaia, A., Taphanel, M. H., Lorre, A., Sinninghe Damsté, J. S., et al. (2010). Distributions and carbon isotopic compositions of lipid biomarkers in authigenic carbonate crusts from the Nordic margin (Norwegian Sea). *Org. Geochem.* 41 (9), 885–890. doi:10.1016/j.orggeochem.2010.03.012

Collister, J. W., Rieley, G., Stern, B., Eglinton, G., and Fry, B. (1994). Compound-specific δ^{13}C analyses of leaf lipids from plants with differing carbon dioxide metabolisms. *Org. Geochem.* 21 (6-7), 619–627. doi:10.1016/0146-6380(94)90008-6

Comita, P. B., Gagosian, R. B., Pang, H., and Costello, C. E. (1984). Structural elucidation of a unique macrocyclic membrane lipid from a new, extremely thermophilic, deep-sea hydrothermal vent archaebacterium, *Methanococcus jannaschii*. *J. Biol. Chem.* 259 (24), 15234–15241. doi:10.1016/S0021-9258(17)42540-3

Davis, J. B., and Kirkland, D. W. (1970). Native sulfur deposition in the castile formation, culberson county, Texas. *Econ. Geol.* 65 (2), 107–121. doi:10.2113/gsecongeo.65.2.107

Dawson, K. S., Freeman, K. H., and Macalady, J. L. (2012). Molecular characterization of core lipids from halophilic archaea grown under different salinity conditions. *Org. Geochem.* 48, 1–8. doi:10.1016/j.orggeochem.2012.04.003

de Galdeano, C. S. (1990). Geologic evolution of the betic cordilleras in the western mediterranean, Miocene to the present. *Tectonophysics* 172 (1-2), 107–119. doi:10.1016/0040-1951(90)90062-D

de Lange, G. J., and Krijgsman, W. (2010). Messinian salinity crisis: A novel unifying shallow gypsum/deep dolomite formation mechanism. *Mar. Geol.* 275 (1-4), 273–277. doi:10.1016/j.margeo.2010.05.003

Decho, A. W. (1990). "Microbial exopolymer secretions in ocean environments: Their role (s) in food webs and marine processes," in *Oceanography and marine biology: An annual review*. Editor H. Barnes (Aberdeen: Aberdeen University Press), 73–153.

Dessau, G., Jensen, M. L., and Nakai, N. (1962). Geology and isotopic studies of Sicilian sulfur deposits. *Econ. Geol.* 57 (3), 410–438. doi:10.2113/gsecongeo.57.3.410

Detmers, J., Brüchert, V., Habicht, K. S., and Kuever, J. (2001). Diversity of sulfur isotope fractionations by sulfate-reducing prokaryotes. *Appl. Environ. Microbiol.* 67 (2), 888–894. doi:10.1128/AEM.67.2.888-894.2001

Didyk, B. M., Simoneit, B. R. T., Brassell, S. T., and Eglinton, G. (1978). Organic geochemical indicators of palaeoenvironmental conditions of sedimentation. *Nature* 272 (5650), 216–222. doi:10.1038/272216a0

Drake, H., Åström, M. E., Heim, C., Broman, C., Åström, J., Whitehouse, M., et al. (2015). Extreme ^{13}C-depletion of carbonates formed during oxidation of biogenic methane in fractured granite. *Nat. Commun.* 6 (1), 7020–7029. doi:10.1038/ncomms8020

Eglinton, T. I., and Eglinton, G. (2008). Molecular proxies for paleoclimatology. *Earth Planet. Sci. Lett.* 275 (1-2), 1–16. doi:10.1016/j.epsl.2008.07.012

Elvert, M., Boetius, A., Knittel, K., and Jørgensen, B. B. (2003). Characterization of specific membrane fatty acids as chemotaxonomic markers for sulfate-reducing bacteria involved in anaerobic oxidation of methane. *Geomicrobiol. J.* 20 (4), 403–419. doi:10.1080/01490450303894

Elvert, M., Suess, E., and Whiticar, M. J. (1999). Anaerobic methane oxidation associated with marine gas hydrates: Superlight C-isotopes from saturated and unsaturated C_{20} and C_{25} irregular isoprenoids. *Naturwissenschaften* 86 (6), 295–300. doi:10.1007/s001140050619

Feely, H. W., and Kulp, J. L. (1957). Origin of Gulf Coast salt-dome sulphur deposits. *AAPG Bull.* 41 (8), 1802–1853. doi:10.1306/0BDA5939-16BD-11D7-8645000102C1865D

Fernandes, T. A., Iyer, V., and Apte, S. K. (1993). Differential effects of salt and osmotic stress on growth and nitrogen fixation in *Anabaena* sp. strain L-31. *Appl. Environ. Microbiol.* 59, 899–904. doi:10.1128/aem.59.3.899-904.1993

Fitz, R. M., and Cypionka, H. (1990). Formation of thiosulfate and trithionate during sulfite reduction by washed cells of *Desulfovibrio desulfuricans*. *Archives Microbiol.* 154 (4), 400–406. doi:10.1007/BF00276538

Flügel, E. (2004). *Microfacies of carbonate rocks*. Berlin: Springer-Verlag, 976.

Fossing, H., and Jørgensen, B. B. (1989). Measurement of bacterial sulfate reduction in sediments: Evaluation of a single-step chromium reduction method. *Biogeochemistry* 8 (3), 205–222. doi:10.1007/BF00002889

Füchtbauer, H. (1988). *Sedimente und Sedimentgesteine*. Stuttgart: Schweizerbart.

Garcia-Veigas, J., Orti, F., Rosell, L., Ayora, C., Rouchy, J. M., and Lugli, S. (1995). The Messinian salt of the Mediterranean: Geochemical study of the salt from the central Sicily Basin and comparison with the Lorca Basin (Spain). *Bull. Société Géologique Fr.* 166 (6), 699–710.

García-Veigas, J., Ortí, F., Rosell, L., and Ingles, M. (1994). Caracterizacion petrologica y geoquimica de la unidad salina messiniense de la cuenca de Lorca (sondeos S4 y S5). *Geogaceta* 15, 78–81.

García-Veigas, J., Gibert, L., Cendón, D. I., Artiaga, D., Corbí, H., Soria, J. M., et al. (2020). Late Miocene evaporite geochemistry of Lorca and Fortuna basins (eastern betics, SE Spain): Evidence of restriction and continentalization. *Basin Res.* 32 (5), 916–948. doi:10.1111/bre.12408

Geng, L., Savarino, J., Savarino, C. A., Caillon, N., Cartigny, P., Hattori, S., et al. (2018). A simple and reliable method reducing sulfate to sulfide for multiple sulfur isotope analysis. *Rapid Commun. Mass Spectrom.* 32 (4), 333–341. doi:10.1002/rcm.8048

Gill, B. C., Lyons, T. W., and Frank, T. D. (2008). Behavior of carbonate-associated sulfate during meteoric diagenesis and implications for the sulfur isotope paleoproxy. *Geochimica Cosmochimica Acta* 72 (19), 4699–4711. doi:10.1016/j.gca.2008.07.001

Gischler, E., Birgel, D., Brunner, B., and Peckmann, J. (2020). Microbialite occurrence and patterns in holocene reefs of Bora Bora, Society Islands. *Palaios* 35 (6), 262–276. doi:10.2110/palo.2020.026

Grice, K., Schouten, S., Nissenbaum, A., Charrach, J., and Sinninghe Damsté, J. S. (1998). Isotopically heavy carbon in the C_{21} to C_{25} regular isoprenoids in halite-rich deposits from the Sdom Formation, Dead Sea Basin, Israel. *Org. Geochem.* 28 (6), 349–359. doi:10.1016/S0146-6380(98)00006-0

Grossi, V., Beker, B., Geenevasen, J. A. J., Schouten, S., Raphel, D., Fontaine, M.-F., et al. (2004). C_{25} highly branched isoprenoid alkenes from the marine benthic diatom *Pleurosigma strigosum*. *Phytochemistry* 65 (22), 3049–3055. doi:10.1016/j.phytochem.2004.09.002

Grossi, V., Mollex, D., Vinçon-Laugier, A., Hakil, F., Pacton, M., and Cravo-Laureau, C. (2015). Mono-and dialkyl glycerol ether lipids in anaerobic bacteria: Biosynthetic insights from the mesophilic sulfate reducer *Desulfatibacillum alkenivorans* PF2803T. *Appl. Environ. Microbiol.* 81 (9), 3157–3168. doi:10.1128/AEM.03794-14

Gründger, F., Carrier, V., Svenning, M. M., Panieri, G., Vonnahme, T. R., Klasek, S., et al. (2019). Methane-fuelled biofilms predominantly composed of methanotrophic ANME-1 in Arctic gas hydrate-related sediments. *Sci. Rep.* 9, 9725. doi:10.1038/s41598-019-46209-5

Habicht, K. S., and Canfield, D. E. (1997). Sulfur isotope fractionation during bacterial sulfate reduction in organic-rich sediments. *Geochimica Cosmochimica Acta* 61 (24), 5351–5361. doi:10.1016/S0016-7037(97)00311-6

Hayes, J. M. (1993). Factors controlling ^{13}C contents of sedimentary organic compounds: Principles and evidence. *Mar. Geol.* 113 (1-2), 111–125. doi:10.1016/0025-3227(93)90153-M

Heindel, K., Birgel, D., Brunner, B., Thiel, V., Westphal, H., Gischler, E., et al. (2012). Post-glacial microbialite formation in coral reefs of the Pacific, Atlantic, and Indian Oceans. *Chem. Geol.* 304-305, 117–130. doi:10.1016/j.chemgeo.2012.02.009

Heindel, K., Birgel, D., Peckmann, J., Kuhnert, H., and Westphal, H. (2010). Formation of deglacial microbialites in coral reefs off Tahiti (IODP 310) involving sulfate-reducing bacteria. *Palaios* 25 (10), 618–635. doi:10.2110/palo.2010.p10-032r

Hinrichs, K.-U., Hayes, J. M., Sylva, S. P., Brewer, P. G., and DeLong, E. F. (1999). Methane-consuming archaebacteria in marine sediments. *Nature* 398 (6730), 802–805. doi:10.1038/19751

Hinrichs, K.-U., Summons, R. E., Orphan, V., Sylva, S. P., and Hayes, J. M. (2000). Molecular and isotopic analysis of anaerobic methane-oxidizing communities in marine sediments. *Org. Geochem.* 31 (12), 1685–1701. doi:10.1016/S0146-6380(00)00106-6

Huang, W. Y., and Meinschein, W. G. (1979). Sterols as ecological indicators. *Geochimica Cosmochimica Acta* 43 (5), 739–745. doi:10.1016/0016-7037(79)90257-6

Hunt, W. F. (1915). The origin of the sulphur deposits of Sicily. *Econ. Geol.* 10 (6), 543–579. doi:10.2113/gsecongeo.10.6.543

Kaneda, T. (1991). Iso- and anteiso-fatty acids in bacteria: Biosynthesis, function, and taxonomic significance. *Microbiol. Rev.* 55 (2), 288–302. doi:10.1128/mr.55.2.288-302.1991

Kastner, M. (1984). Sedimentology: Control of dolomite formation. *Nature* 311 (5985), 410–411. doi:10.1038/311410b0

Kates, M. (1993). Biology of halophilic bacteria, Part II. Membrane lipids of extreme halophiles: Biosynthesis, function and evolutionary significance. *Experientia* 49 (12), 1027–1036. doi:10.1007/bf01929909

Kevorkian, R. T., Callahan, S., Winstead, R., and Lloyd, K. G. (2021). ANME-1 archaea may drive methane accumulation and removal in estuarine sediments. *Environ. Microbiol. Rep.* 13 (2), 185–194. doi:10.1111/1758-2229.12926

Kleikemper, J., Schroth, M. H., Bernasconi, S. M., Brunner, B., and Zeyer, J. (2004). Sulfur isotope fractionation during growth of sulfate-reducing bacteria on various carbon sources. *Geochimica Cosmochimica Acta* 68 (23), 4891–4904. doi:10.1016/j.gca.2004.05.034

Koga, Y., Morii, H., Akagawa-Matsushita, M., and Ohga, M. (1998). Correlation of polar lipid composition with 16S rRNA phylogeny in methanogens. Further analysis of lipid component parts. *Biosci. Biotechnol. Biochem.* 62 (2), 230–236. doi:10.1271/bbb.62.230

Kok, M. D., Rijpstra, W. I. C., Robertson, L., Volkman, J. K., and Sinninghe Damsté, J. S. (2000). Early steroid sulfurisation in surface sediments of a permanently stratified lake (Ace Lake, Antarctica). *Geochimica Cosmochimica Acta* 64 (8), 1425–1436. doi:10.1016/S0016-7037(99)00430-5

Krake, N., Birgel, D., Smrzka, D., Zwicker, J., Huang, H., Feng, D., et al. (2022). Molecular and isotopic signatures of oil-driven bacterial sulfate reduction at seeps in the southern Gulf of Mexico. *Chem. Geol.* 595, 120797. doi:10.1016/j.chemgeo.2022.120797

Krause, S., Liebetrau, V., Gorb, S., Sánchez-Román, M., McKenzie, J. A., and Treude, T. (2012). Microbial nucleation of Mg-rich dolomite in exopolymeric substances under anoxic modern seawater salinity: New insight into an old enigma. *Geology* 40 (7), 587–590. doi:10.1130/G32923.1

Krijgsman, W., Garcés, M., Agustı, J., Raffi, I., Taberner, C., and Zachariasse, W. J. (2000). The 'Tortonian salinity crisis' of the eastern Betics (Spain). *Earth Planet. Sci. Lett.* 181 (4), 497–511. doi:10.1016/S0012-821X(00)00224-7

Kutuzov, I., Rosenberg, Y. O., Bishop, A., and Amrani, A. (2020). "The origin of organic sulphur compounds and their impact on the paleoenvironmental record," in *Hydrocarbons, oils and lipids: Diversity, origin, chemistry and fate*. Editor H. Wilkes (Cham: Springer), 355–408. doi:10.1007/978-3-319-90569-3_1

Labidi, J., Cartigny, P., Birck, J. L., Assayag, N., and Bourrand, J. J. (2012). Determination of multiple sulfur isotopes in glasses: A reappraisal of the morb δ^{34}S. *Chem. Geol.* 334, 189–198. doi:10.1016/j.chemgeo.2012.10.028

Labrado, A. L., Brunner, B., Bernasconi, S. M., and Peckmann, J. (2019). Formation of large native sulfur deposits does not require molecular oxygen. *Front. Microbiol.* 10, 24. doi:10.3389/fmicb.2019.00024

Lindtke, J., Ziegenbalg, S. B., Brunner, B., Rouchy, J. M., Pierre, C., and Peckmann, J. (2011). Authigenesis of native sulphur and dolomite in a lacustrine evaporitic setting (Hellín basin, Late Miocene, SE Spain). *Geol. Mag.* 148 (4), 655–669. doi:10.1017/S0016756811000124

Lippmann, F. (1973). "Crystal chemistry of sedimentary carbonate minerals," in *Sedimentary carbonate minerals* (Berlin, Heidelberg: Springer), 5–96. doi:10.1007/978-3-642-65474-9_2

Liu, R., Shan, Y., Xi, S., Zhang, X., and Sun, C. (2022). A deep-sea sulfate-reducing bacterium generates zero-valent sulfur via metabolizing thiosulfate. *mLife* 1, 257–271. doi:10.1002/mlf2.12038

Liu, X. L., Birgel, D., Elling, F. J., Sutton, P. A., Lipp, J. S., Zhu, R., et al. (2016). From ether to acid: A plausible degradation pathway of glycerol dialkyl glycerol tetraethers. *Geochimica Cosmochimica Acta* 183, 138–152. doi:10.1016/j.gca.2016.04.016

Londry, K. L., Dawson, K. G., Grover, H. D., Summons, R. E., and Bradley, A. S. (2008). Stable carbon isotope fractionation between substrates and products of *Methanosarcina barkeri*. *Org. Geochem.* 39 (5), 608–621. doi:10.1016/j.orggeochem.2008.03.002

Londry, K. L., and Des Marais, D. J. (2003). Stable carbon isotope fractionation by sulfate-reducing bacteria. *Appl. Enviromental Microbiol.* 69 (5), 2942–2949. doi:10.1128/AEM.69.5.2942-2949.2003

Londry, K. L., Jahnke, L. L., and Des Marais, D. J. (2004). Stable carbon isotope ratios of lipid biomarkers of sulfate-reducing bacteria. *Appl. Environ. Microbiol.* 70 (2), 745–751. doi:10.1128/AEM.70.2.745-751.2004

Lu, Y., Sun, X., Xu, H., Konishi, H., Lin, Z., Xu, L., et al. (2018). Formation of dolomite catalyzed by sulfate-driven anaerobic oxidation of methane: Mineralogical and geochemical evidence from the northern South China Sea. *Am. Mineralogist* 103 (5), 720–734. doi:10.2138/am-2018-6226

Lu, Y., Yang, X., Lin, Z., Sun, X., Yang, Y., and Peckmann, J. (2021). Reducing microenvironments promote incorporation of magnesium ions into authigenic carbonate forming at methane seeps: Constraints for dolomite formation. *Sedimentology* 68 (7), 2945–2964. doi:10.1111/sed.12919

Machel, H. G. (2001). Bacterial and thermochemical sulfate reduction in diagenetic settings – old and new insights. *Sediment. Geol.* 140 (1-2), 143–175. doi:10.1016/S0037-0738(00)00176-7

Machel, H. G., Krouse, H. R., and Sassen, R. (1995). Products and distinguishing criteria of bacterial and thermochemical sulfate reduction. *Appl. Geochem.* 10 (4), 373–389. doi:10.1016/0883-2927(95)00008-8

Machel, H. G. (1992). "Low-temperature and high-temperature origins of elemental sulfur in diagenetic environments," in *Native sulfur – developments in geology and exploration*. Editors G. R. Wessel, B. H. Wimberly, and Littleton (United States: CO: Society for Mining, Metallurgy, and Exploration), 3–22.

Markham, G. D., Glusker, J. P., and Bock, C. W. (2002). The arrangement of first-and second-sphere water molecules in divalent magnesium complexes: Results from molecular orbital and density functional theory and from structural crystallography. *J. Phys. Chem. B* 106 (19), 5118–5134. doi:10.1021/jp020078x

McCaffrey, M. A., Farrington, J. W., and Repeta, D. J. (1989). Geochemical implications of the lipid composition of *Thioploca* spp. from the Peru upwelling region-15°S. *Org. Geochem.* 14 (1), 61–68. doi:10.1016/0146-6380(89)90019-3

McGenity, T. J., and Sorokin, D. Y. (2018). "Methanogens and methanogenesis in hypersaline environments," in *Biogenesis of hydrocarbons. Handbook of hydrocarbon and lipid microbiology*. Editors A. Stams and D. Sousa (Cham: Springer), 1–27. doi:10.1007/978-3-319-53114-4_12-1

Milucka, J., Ferdelman, T. G., Polerecky, L., Franzke, D., Wegener, G., Schmid, M., et al. (2012). Zero-valent sulphur is a key intermediate in marine methane oxidation. *Nature* 491 (7425), 541–546. doi:10.1038/nature11656

Miyajima, Y., Watanabe, Y., Goto, A. S., Jenkins, R. G., Sakai, S., Matsumoto, R., et al. (2020). Archaeal lipid biomarker as a tool to constrain the origin of methane at ancient methane seeps: Insight into subsurface fluid flow in the geological past. *J. Asian Earth Sci.* 189, 104134. doi:10.1016/j.jseaes.2019.104134

Naafs, B. D. A., Hefter, J., Acton, G., Haug, G. H., Martínez-Garcia, A., Pancost, R., et al. (2012). Strengthening of north American dust sources during the late Pliocene (2.7 ma). *Earth Planet. Sci. Lett.* 317, 8–19. doi:10.1016/j.epsl.2011.11.026

Natalicchio, M., Birgel, D., Dela Pierre, F., Ziegenbalg, S., Hoffmann-Sell, L., Gier, S., et al. (2022). Messinian bottom-grown selenitic gypsum: An archive of microbial life. *Geobiology* 20 (1), 3–21. doi:10.1111/gbi.12464

Natalicchio, M., Pellegrino, L., Clari, P., Pastero, L., and Pierre, F. D. (2021). Gypsum lithofacies and stratigraphic architecture of a Messinian marginal basin (Piedmont Basin, NW Italy). *Sediment. Geol.* 425, 106009. doi:10.1016/j.sedgeo.2021.106009

Nauhaus, K., Treude, T., Boetius, A., and Krüger, M. (2005). Environmental regulation of the anaerobic oxidation of methane: A comparison of ANME-I and ANME-II communities. *Environ. Microbiol.* 7 (1), 98–106. doi:10.1111/j.1462-2920.2004.00669.x

Niemann, H., and Elvert, M. (2008). Diagnostic lipid biomarker and stable carbon isotope signatures of microbial communities mediating the anaerobic oxidation of methane with sulphate. *Org. Geochem.* 39 (12), 1668–1677. doi:10.1016/j.orggeochem.2007.11.003

Ono, S., Wing, B., Johnston, D., Farquhar, J., and Rumble, D. (2006). Mass-dependent fractionation of quadruple stable sulfur isotope system as a new tracer of sulfur biogeochemical cycles. *Geochimica Cosmochimica Acta* 70 (9), 2238–2252. doi:10.1016/j.gca.2006.01.022

Oren, A. (1999). Bioenergetic aspects of halophilism. *Microbiol. Mol. Biol. Rev.* 63 (2), 334–348. doi:10.1128/MMBR.63.2.334-348.1999

Oren, A. (2013). Life at high salt concentrations, intracellular KCl concentrations, and acidic proteomes. *Front. Microbiol.* 4, 315. doi:10.3389/fmicb.2013.00315

Orphan, V. J., House, C. H., Hinrichs, K.-U., McKeegan, K. D., and DeLong, E. F. (2001). Methane-consuming archaea revealed by directly coupled isotopic and phylogenetic analysis. *Science* 293 (5529), 484–487. doi:10.1126/science.1061338

Orphan, V. J., House, C. H., Hinrichs, K.-U., McKeegan, K. D., and DeLong, E. F. (2002). Multiple archaeal groups mediate methane oxidation in anoxic cold seep sediments. *Proc. Natl. Acad. Sci.* 99 (11), 7663–7668. doi:10.1073/pnas.072210299

Pancost, R. D., and Pagani, M. (2006). "Controls on the carbon isotopic compositions of lipids in marine environments," in *Marine organic matter: Biomarkers, isotopes and DNA. The handbook of environmental chemistry*. Editor J. K. Volkman (Berlin, Heidelberg: Springer), 209–239. doi:10.1007/698_2_007

Pancost, R. D., Sinninghe Damsté, J. S., de Lint, S., van der Maarel, M. J., Gottschal, J. C., and Medinaut Shipboard Scientific Party (2000). Biomarker evidence for widespread anaerobic methane oxidation in Mediterranean sediments by a consortium of methanogenic archaea and bacteria. *Appl. Environ. Microbiol.* 66 (3), 1126–1132. doi:10.1128/AEM.66.3.1126-1132.2000

Parshina, S. N., Sipma, J., Nakashimada, Y., Henstra, A. M., Smidt, H., Lysenko, A. M., et al. (2005). *Desulfotomaculum carboxydivorans* sp. nov., a novel sulfate-reducing bacterium capable of growth at 100% CO. *Int. J. Syst. Evol. Microbiol.* 55 (5), 2159–2165. doi:10.1099/ijs.0.63780-0

Peckmann, J., Paul, J., and Thiel, V. (1999). Bacterially mediated formation of diagenetic aragonite and native sulfur in Zechstein carbonates (Upper Permian, Central Germany). *Sediment. Geol.* 126 (1-4), 205–222. doi:10.1016/S0037-0738(99)00041-X

Peckmann, J., and Thiel, V. (2004). Carbon cycling at ancient methane–seeps. *Chem. Geol.* 205 (3-4), 443–467. doi:10.1016/j.chemgeo.2003.12.025

Permanyer, A., Jorge, R., Baudino, R., and Gibert, L. (2016). Organic-rich shales from internal betic basins (SE Spain): Potential source rocks analogs for the pre-Messinian salt play in the Western Mediterranean. *Geol. Acta* 14 (4), 443–460. doi:10.1344/GeologicaActa2016.14.4.7

Petrash, D. A., Bialik, O. M., Bontognali, T. R., Vasconcelos, C., Roberts, J. A., McKenzie, J. A., et al. (2017). Microbially catalyzed dolomite formation: From near-surface to burial. *Earth-Science Rev.* 171, 558–582. doi:10.1016/j.earscirev.2017.06.015

Pineda, V., Gibert, L., Soria, J. M., Carrazana, A., Ibáñez-Insa, J., and Sánchez-Román, M. (2021). Interevaporitic deposits of Las Minas gypsum unit: A record of late Tortonian marine incursions and dolomite precipitation in Las Minas basin (eastern betic Cordillera, SE Spain). *Palaeogeogr. Palaeoclimatol. Palaeoecol.* 564, 110171. doi:10.1016/j.palaeo.2020.110171

Playà, E., Ortı, F., and Rosell, L. (2000). Marine to non-marine sedimentation in the upper Miocene evaporites of the eastern betics, SE Spain: Sedimentological and geochemical evidence. *Sediment. Geol.* 133 (1-2), 135–166. doi:10.1016/S0037-0738(00)00033-6

Powell, T. G., and McKirdy, D. M. (1973). Relationship between ratio of pristane to phytane, crude oil composition and geological environment in Australia. *Nat. Phys. Sci.* 243 (124), 37–39. doi:10.1038/physci243037a0

Repeta, D. J., Simpson, D. J., Jørgensen, B. B., and Jannasch, H. W. (1989). Evidence for anoxygenic photosynthesis from the distribution of bacterio-chlorophylls in the Black Sea. *Nature* 342 (6245), 69–72. doi:10.1038/342069a0

Rossel, P. E., Elvert, M., Ramette, A., Boetius, A., and Hinrichs, K.-U. (2011). Factors controlling the distribution of anaerobic methanotrophic communities in marine environments: Evidence from intact polar membrane lipids. *Geochimica Cosmochimica Acta* 75 (1), 164–184. doi:10.1016/j.gca.2010.09.031

Rossel, P. E., Lipp, J. S., Fredricks, H. F., Arnds, J., Boetius, A., Elvert, M., et al. (2008). Intact polar lipids of anaerobic methanotrophic archaea and associated bacteria. *Org. Geochem.* 39 (8), 992–999. doi:10.1016/j.orggeochem.2008.02.021

Rouchy, J. M. (1982). *La Genèse des Évaporites Messiniennes de Méditerranée*. Mémoires du Muséum National d'Histoire Naturelle, Série C, Édition du Muséum.

Rouchy, J. M., Taberner, C., Blanc-Valleron, M. M., Sprovieri, R., Russell, M., Pierre, C., et al. (1998). Sedimentary and diagenetic markers of the restriction in a marine basin: The Lorca Basin (SE Spain) during the messinian. *Sediment. Geol.* 121 (1-2), 23–55. doi:10.1016/S0037-0738(98)00071-2

Roveri, M., Flecker, R., Krijgsman, W., Lofi, J., Lugli, S., Manzi, V., et al. (2014). The Messinian salinity crisis: Past and future of a great challenge for marine sciences. *Mar. Geol.* 352, 25–58. doi:10.1016/j.margeo.2014.02.002

Rowland, S. J. (1990). Production of acyclic isoprenoid hydrocarbons by laboratory maturation of methanogenic bacteria. *Org. Geochem.* 15 (1), 9–16. doi:10.1016/0146-6380(90)90181-X

Russell, M., Grimalt, J. O., Hartgers, W. A., Taberner, C., and Rouchy, J. M. (1997). Bacterial and algal markers in sedimentary organic matter deposited under natural sulphurization conditions (Lorca Basin, Murcia, Spain). *Org. Geochem.* 26 (9-10), 605–625. doi:10.1016/S0146-6380(97)00034-X

Russell, M., Hartgers, W. A., and Grimalt, J. O. (2000). Identification and geochemical significance of sulphurized fatty acids in sedimentary organic matter from the Lorca Basin, SE Spain. *Geochim. Cosmochim. Acta.* 64 (21), 3711–3723. doi:10.1016/S0016-7037(00)00470-1

Sabino, M., Pierre, F. D., Natalicchio, M., Birgel, D., Gier, S., and Peckmann, J. (2021). The response of water column and sedimentary environments to the advent of the

Messinian salinity crisis: Insights from an onshore deep-water section (govone, NW Italy). *Geol. Mag.* 158 (5), 825–841. doi:10.1017/S0016756820000874

Sabino, M., Schefuß, E., Natalicchio, M., Pierre, F. D., Birgel, D., Bortels, D., et al. (2020). Climatic and hydrologic variability in the northern Mediterranean across the onset of the Messinian salinity crisis. *Palaeogeogr. Palaeoclimatol. Palaeoecol.* 545, 109632. doi:10.1016/j.palaeo.2020.109632

Sala, D., Grossi, V., Agogué, H., Leboulanger, C., Jézéquel, G., Antheaume, I., et al. (2021). Influence of aphotic haloclines and euxinia on organic biomarkers and microbial communities in a thalassohaline and alkaline volcanic crater lake. *Geobiology* 20 (2), 292–309. doi:10.1111/gbi.12477

Schouten, S., Van Der Maarel, M. J., Huber, R., and Sinninghe Damsté, J. S. (1997). 2,6,10,15,19-Pentamethylicosenes in *Methanolobus bombayensis*, a marine methanogenic archaeon, and in *Methanosarcina mazei*. *Org. Geochem.* 26 (5-6), 409–414. doi:10.1016/S0146-6380(97)00011-9

Schouten, S., Wakeham, S. G., Hopmans, E. C., and Sinninghe Damsté, J. S. (2003). Biogeochemical evidence that thermophilic archaea mediate the anaerobic oxidation of methane. *Appl. Environ. Microbiol.* 69 (3), 1680–1686. doi:10.1128/AEM.69.3.1680-1686.2003

Sharma, T., and Clayton, R. N. (1965). Measurement of O^{18}/O^{16} ratios of total oxygen of carbonates. *Geochimica Cosmochimica Acta* 29 (12), 1347–1353. doi:10.1016/0016-7037(65)90011-6

Sim, M. S., Bosak, T., and Ono, S. (2011). Large sulfur isotope fractionation does not require disproportionation. *Science* 333 (6038), 74–77. doi:10.1126/science.1205103

Sinninghe Damsté, J. S., and De Leeuw, J. W. (1990). Analysis, structure and geochemical significance of organically-bound sulphur in the geosphere: State of the art and future research. *Org. Geochem.* 16 (4-6), 1077–1101. doi:10.1016/0146-6380(90)90145-P

Sinninghe Damsté, J. S., Kenig, F., Koopmans, M. P., Köster, J., Schouten, S., Hayes, J. M., et al. (1995). Evidence for gammacerane as an indicator of water column stratification. *Geochimica Cosmochimica Acta* 59 (9), 1895–1900. doi:10.1016/0016-7037(95)00073-9

Sinninghe Damsté, J. S., Rijpstra, W. I. C., Coolen, M. J., Schouten, S., and Volkman, J. K. (2007). Rapid sulfurisation of highly branched isoprenoid (HBI) alkenes in sulfidic Holocene sediments from Ellis Fjord, Antarctica. *Org. Geochem.* 38 (1), 128–139. doi:10.1016/j.orggeochem.2006.08.003

Sinninghe Damsté, J. S., and Rijpstra, W. I. C. (1993). Identification of a novel C_{25} highly branched isoprenoid thiophene in sediments. *Org. Geochem.* 20 (3), 327–331. doi:10.1016/0146-6380(93)90122-R

Sinninghe Damsté, J. S., Schouten, S., Rijpstra, W. I. C., Hopmans, E. C., Peletier, H., Gieskes, W. W., et al. (1999). Structural identification of the C_{25} highly branched isoprenoid pentaene in the marine diatom *Rhizosolenia setigera*. *Org. Geochem.* 30 (12), 1581–1583. doi:10.1016/S0146-6380(99)00140-0

Smrzka, D., Zwicker, J., Kolonic, S., Birgel, D., Little, C. T., Marzouk, A. M., et al. (2017). Methane seepage in a Cretaceous greenhouse world recorded by an unusual carbonate deposit from the Tarfaya Basin, Morocco. *Depositional Rec.* 3 (1), 4–37. doi:10.1002/dep2.24

Sorokin, D. Y., Diender, M., Merkel, A. Y., Koenen, M., Bale, N. J., Pabst, M., et al. (2021). *Natranaerofaba carboxydovora* gen. nov., sp. nov., an extremely haloalkaliphilic CO-utilizing acetogen from a hypersaline soda lake representing a novel deep phylogenetic lineage in the class '*Natranaerobiia*. *Environ. Microbiol.* 23 (7), 3460–3476. doi:10.1111/1462-2920.15241

Spring, S., Sorokin, D. Y., Verbarg, S., Rohde, M., Woyke, T., and Kyrpides, N. C. (2019). Sulfate-reducing bacteria that produce exopolymers thrive in the calcifying zone of a hypersaline cyanobacterial mat. *Front. Microbiol.* 10, 862. doi:10.3389/fmicb.2019.00862

Stackebrandt, E. (2014). "The emended family Peptococcaceae and description of the families Desulfitobacteriaceae, Desulfotomaculaceae, and Thermincolaceae," in *The prokaryotes*. Editors E. Rosenberg, E. F. DeLong, S. Lory, E. Stackebrandt, and F. Thompson (Berlin, Heidelberg: Springer), 285–290. doi:10.1007/978-3-642-30120-9_364

Sutherland, I. W. (2001). Exopolysaccharides in biofilms, flocs and related structures. *Water Sci. Technol.* 43 (6), 77–86. doi:10.2166/wst.2001.0345

Taylor, J., and Parkes, R. J. (1983). The cellular fatty acids of the sulphate-reducing bacteria, *Desulfobacter* sp., *Desulfobulbus* sp. and *Desulfovibrio desulfuricans*. *Microbiology* 129 (11), 3303–3309. doi:10.1099/00221287-129-11-3303

Teixidor, P., Grimait, J. O., Pueyo, J. J., and Rodriguez-Valera, F. (1993). Isopranylglycerol diethers in non-alkaline evaporitic environments. *Geochimica Cosmochimica Acta* 57 (18), 4479–4489. doi:10.1016/0016-7037(93)90497-K

Teske, A., Hinrichs, K.-U., Edgcomb, V., de Vera Gomez, A., Kysela, D., Sylva, S. P., et al. (2002). Microbial diversity of hydrothermal sediments in the Guaymas Basin: Evidence for anaerobic methanotrophic communities. *Appl. Environ. Microbiol.* 68 (4), 1994–2007. doi:10.1128/AEM.68.4.1994-2007.2002

Thiel, V., Blumenberg, M., Pape, T., Seifert, R., and Michaelis, W. (2003). Unexpected occurrence of hopanoids at gas seeps in the Black Sea. *Org. Geochem.* 34 (1), 81–87. doi:10.1016/S0146-6380(02)00191-2

Thiel, V. (2020). "Methane carbon cycling in the past: Insights from hydrocarbon and lipid biomarkers," in *Hydrocarbons, oils and lipids: Diversity, origin, chemistry and fate. Handbook of hydrocarbon and lipid microbiology*. Editor H. Wilkes (Cham: Springer), 781–810. doi:10.1007/978-3-319-90569-3_6

Thiel, V., Peckmann, J., Seifert, R., Wehrung, P., Reitner, J., and Michaelis, W. (1999). Highly isotopically depleted isoprenoids: Molecular markers for ancient methane venting. *Geochimica Cosmochimica Acta* 63, 3959–3966. doi:10.1016/S0016-7037(99)00177-5

Thioye, A., Gam, Z. B. A., Mbengue, M., Cayol, J. L., Joseph-Bartoli, M., Touré-Kane, C., et al. (2017). *Desulfovibrio senegalensis* sp. nov., a mesophilic sulfate reducer isolated from marine sediment. *Int. J. Syst. Evol. Microbiol.* 67 (9), 3162–3166. doi:10.1099/ijsem.0.001997

Tornabene, T. G., Langworthy, T. A., Holzer, G., and Oro, J. (1979). Squalenes, phytanes and other isoprenoids as major neutral lipids of methanogenic and thermoacidophilic "archaebacteria". *J. Mol. Evol.* 13 (1), 73–83. doi:10.1007/BF01732755

Tourte, M., Schaeffer, P., Grossi, V., and Oger, P. M. (2020). Functionalized membrane domains: An ancestral feature of Archaea? *Front. Microbiol.* 11, 526. doi:10.3389/fmicb.2020.00526

Valisolalao, J., Perakis, N., Chappe, B., and Albrecht, P. (1984). A novel sulfur containing C_{35} hopanoid in sediments. *Tetrahedron Lett.* 25 (11), 1183–1186. doi:10.1016/S0040-4039(01)91555-2

van Gemerden, H., and Mas, J. (1995). "Ecology of phototrophic sulfur bacteria," in *Anoxygenic photosynthetic bacteria*. Editors R. E. Blankenship, M. T. Madigan, and C. E. Bauer (Dordrecht: Springer), 49–85. doi:10.1007/0-306-47954-0_4

Vandier, F., Tourte, M., Doumbe-Kingue, C., Plancq, J., Schaeffer, P., Oger, P., et al. (2021). Reappraisal of archaeal C_{20}-C_{25} diether lipid (extended archaeol) origin and use as a biomarker of hypersalinity. *Org. Geochem.* 159, 104276. doi:10.1016/j.orggeochem.2021.104276

Vinçon-Laugier, A., Cravo-Laureau, C., Mitteau, I., and Grossi, V. (2017). Temperature-dependent alkyl glycerol ether lipid composition of mesophilic and thermophilic sulfate-reducing bacteria. *Front. Microbiol.* 8, 1532. doi:10.3389/fmicb.2017.01532

Vinçon-Laugier, A., Grossi, V., Pacton, M., Escarguel, G., and Cravo-Laureau, C. (2016). The alkyl glycerol ether lipid composition of heterotrophic sulfate reducing bacteria strongly depends on growth substrate. *Org. Geochem.* 98, 141–154. doi:10.1016/j.orggeochem.2016.05.015

Volkman, J. K. (1986). A review of sterol markers for marine and terrigenous organic matter. *Org. Geochem.* 9 (2), 83–99. doi:10.1016/0146-6380(86)90089-6

Volkman, J. K., Barrett, S. M., and Dunstan, G. A. (1994). C_{25} and C_{30} highly branched isoprenoid alkenes in laboratory cultures of two marine diatoms. *Org. Geochem.* 21 (3-4), 407–414. doi:10.1016/0146-6380(94)90202-X

Wakeham, S. G., Amann, R., Freeman, K. H., Hopmans, E. C., Jørgensen, B. B., Putnam, I. F., et al. (2007). Microbial ecology of the stratified water column of the Black Sea as revealed by a comprehensive biomarker study. *Org. Geochem.* 38 (12), 2070–2097. doi:10.1016/j.orggeochem.2007.08.003

Wakeham, S. G., Sinninghe Damsté, J. S., Kohnen, M. E., and De Leeuw, J. W. (1995). Organic sulfur compounds formed during early diagenesis in Black Sea sediments. *Geochimica Cosmochimica Acta* 59 (3), 521–533. doi:10.1016/0016-7037(94)00361-O

Wakeham, S. G., Turich, C., Schubotz, F., Podlaska, A., Li, X. N., Varela, R., et al. (2012). Biomarkers, chemistry and microbiology show chemoautotrophy in a multilayer chemocline in the Cariaco Basin. *Deep Sea Res. Part I Oceanogr. Res. Pap.* 63, 133–156. doi:10.1016/j.dsr.2012.01.005

Wang, J., Megha, and London, E. (2004). Relationship between sterol/steroid structure and participation in ordered lipid domains (lipid rafts): Implications for lipid raft structure and function. *Biochemistry* 43(4), 1010–1018. doi:10.1021/bi035696y

Warren, J. (2000). Dolomite: Occurrence, evolution and economically important associations. *Earth-Science Rev.* 52 (1-3), 1–81. doi:10.1016/S0012-8252(00)00022-2

Watanabe, M., Higashioka, Y., Kojima, H., and Fukui, M. (2017). *Desulfosarcina widdelii* sp. nov. and *Desulfosarcina alkanivorans* sp. nov., hydrocarbon-degrading sulfate-reducing bacteria isolated from marine sediment and emended description of the genus *Desulfosarcina*. *Int. J. Syst. Evol. Microbiol.* 67 (8), 2994–2997. doi:10.1099/ijsem.0.002062

Welsh, D. T., Lindsay, Y. E., Caumette, P., Herbert, R. A., and Hannan, J. (1996). Identification of trehalose and glycine betaine as compatible solutes in the moderately halophilic sulfate reducing bacterium, *Desulfovibrio halophilus*. *FEMS Microbiol. Lett.* 140 (2-3), 203–207. doi:10.1111/j.1574-6968.1996.tb08337.x

Werne, J. P., Hollander, D. J., Behrens, A., Schaeffer, P., Albrecht, P., and Sinninghe Damsté, J. S. (2000). Timing of early diagenetic sulfurization of organic matter: A precursor-product relationship in holocene sediments of the anoxic cariaco basin, Venezuela. *Geochimica Cosmochimica Acta* 64 (10), 1741–1751. doi:10.1016/S0016-7037(99)00366-X

Werne, J. P., Hollander, D. J., Lyons, T. W., and Sinninghe Damsté, J. S. (2004). Organic sulfur biogeochemistry: Recent advances and future research directions. *Geol. Soc. Am. Special Pap.* 379, 135–150. doi:10.1130/0-8137-2379-5.135

Whiticar, M. J. (1999). Carbon and hydrogen isotope systematics of bacterial formation and oxidation of methane. *Chem. Geol.* 161 (1-3), 291–314. doi:10.1016/S0009-2541(99)00092-3

Wortmann, U. G., Bernasconi, S. M., and Böttcher, M. E. (2001). Hypersulfidic deep biosphere indicates extreme sulfur isotope fractionation during single-step microbial sulfate reduction. *Geology* 29 (7), 647–650. doi:10.1130/0091-7613(2001)029<0647:HDBIES>2.0.CO;2

Xavier, F., De Las Heras, C., Grimalt, J. O., Lopez, J. F., Albaigés, J., Sinninghe Damsté, J. S. S., et al. (1997). Free and sulphurized hopanoids and highly branched isoprenoids in immature lacustrine oil shales. *Org. Geochem.* 27 (1-2), 41–63. doi:10.1016/s0146-6380(97)00046-6

Xiao, K. Q., Beulig, F., Kjeldsen, K. U., Jørgensen, B. B., and Risgaard-Petersen, N. (2017). Concurrent methane production and oxidation in surface sediment from Aarhus Bay, Denmark. *Front. Microbiol.* 8, 1198. doi:10.3389/fmicb.2017.01198

Xiao, K. Q., Beulig, F., Røy, H., Jørgensen, B. B., and Risgaard-Petersen, N. (2018). Methylotrophic methanogenesis fuels cryptic methane cycling in marine surface sediment. *Limnol. Oceanogr.* 63 (4), 1519–1527. doi:10.1002/lno.10788

Zakharyuk, A. G., Kozyreva, L. P., Khijniak, T. V., Namsaraev, B. B., and Shcherbakova, V. A. (2015). *Desulfonatronum zhilinae* sp. nov., a novel haloalkaliphilic sulfate-reducing bacterium from soda Lake Alginskoe, Trans-Baikal Region, Russia. *Extremophiles* 19 (3), 673–680. doi:10.1007/s00792-015-0747-0

Zhang, C. L., Huang, Z., Cantu, J., Pancost, R. D., Brigmon, R. L., Lyons, T. W., et al. (2005). Lipid biomarkers and carbon isotope signatures of a microbial (*Beggiatoa*) mat associated with gas hydrates in the Gulf of Mexico. *Appl. Environ. Microbiol.* 71 (4), 2106–2112. doi:10.1128/AEM.71.4.2106-2112.2005

Zhang, F., Xu, H., Konishi, H., Kemp, J. M., Roden, E. E., and Shen, Z. (2012). Dissolved sulfide-catalyzed precipitation of disordered dolomite: Implications for the formation mechanism of sedimentary dolomite. *Geochimica Cosmochimica Acta* 97, 148–165. doi:10.1016/j.gca.2012.09.008

Zhang, J., Liu, R., Xi, S., Cai, R., Zhang, X., and Sun, C. (2020). A novel bacterial thiosulfate oxidation pathway provides a new clue about the formation of zero-valent sulfur in deep sea. *ISME J.* 14, 2261–2274. doi:10.1038/s41396-020-0684-5

Zhuang, G. C., Elling, F. J., Nigro, L. M., Samarkin, V., Joye, S. B., Teske, A., et al. (2016). Multiple evidence for methylotrophic methanogenesis as the dominant methanogenic pathway in hypersaline sediments from the Orca Basin, Gulf of Mexico. *Geochimica Cosmochimica Acta* 187, 1–20. doi:10.1016/j.gca.2016.05.005

Ziegenbalg, S. B., Birgel, D., Hoffmann-Sell, L., Pierre, C., Rouchy, J. M., and Peckmann, J. (2012). Anaerobic oxidation of methane in hypersaline Messinian environments revealed by ^{13}C-depleted molecular fossils. *Chem. Geol.* 292, 140–148. doi:10.1016/j.chemgeo.2011.11.024

Ziegenbalg, S. B., Brunner, B., Rouchy, J. M., Birgel, D., Pierre, C., Böttcher, M. E., et al. (2010). Formation of secondary carbonates and native sulphur in sulphate-rich Messinian strata, Sicily. *Sediment. Geol.* 227 (1-4), 37–50. doi:10.1016/j.sedgeo.2010.03.007